UNIVERSITA' DEGLI STUDI DI PADOVA

DIPARTIMENTO DI INGEGNERIA INDUSTRIALE

CORSO DI LAUREA MAGISTRALE IN INGEGNERIA CHIMICA E DEI PROCESSI INDUSTRIALI

Tesi di Laurea Magistrale in
Ingegneria Chimica e dei Processi Industriali

(Laurea di 1° livello DM 270/04)

Design and development of an electrolyte regeneration process for vanadium redox flow batteries

Relatore

Prof. Massimo Guarnieri

Laureando

NICOLA POLI

N° matricola: 1185249

Anno Accademico 2018/2019

Summary

In the present work of thesis, an electrolyte regeneration process for the vanadium redox flow batteries has been analysed. In particular it regards an electrochemical reduction process to rebalance the reduced and oxidised vanadium species in the electrolyte, in order to increase the long cycle life of the battery. The study is divided in two parts: in the first the dynamic response of the battery to this regeneration process has been recorded and through a mathematical model has been justified; in the second an economic analysis has been provided in order to understand the operational and capital costs of the recovery.

Index

Ci sono sempre due scelte nella vita:
accettare le condizioni in cui viviamo o
assumersi la responsabilità di cambiarle.

(Denis Waitley)

Introduction

Vanadium redox flow batteries (VRFBs) represent an alternative solution to store the energy from an intermittent renewable source. Vanadium has four oxidation state: V^{2+}, V^{3+}, V^{4+}, V^{5+} and these ions can be oxidized and reduced through electrochemical reactions. Thanks to these reactions the battery can accumulate or release energy causing them to be charged or discharged. Redox flow batteries are composed of two tanks, where an electrolyte solution is stored, and one stack of cells, where the reactions take place. Each cell is divided in two halves, where the electrode is located: one represents the positive pole and the other one the negative pole. These two half-cells are separated by a membrane which is permeable only for specific ions, such as hydrogen, and it doesn't allow the diffusion of the vanadium ions from one half cell to the other.

Already commercially exploited, the VRFBs exhibit fast response to the power requested from the grid, high efficiency, room temperature operation and an independent sizing between the power released and the energy stored. But their infiltration in the market is made difficult by their high price and their low energy density. Moreover, even though this battery can perform long charge and discharge cycle, its energy capacity can be affected by side reactions which take place into the electrolyte. Therefore, during long-term performance, the VRFB electrolyte is reported to become unbalanced. Imbalance implies an inequality in the amount of oxidized and reduced species in the two tanks and it is usually caused either by vanadium cross-over through the membrane, or by side reactions such as hydrogen evolution or air oxidation of V^{2+} ions in the negative side. While any capacity loss caused by a crossover effect can be readily corrected by simple periodic electrolyte remixing, that rebalances the electrolyte compositions and liquid levels in each reservoir, capacity losses by side reactions can only be corrected by chemical or electrochemical rebalancing of the oxidation state of the two half-cell electrolytes.

The Fraunhofer Institut für Chemische Technologie in Pfinztal, which has been working on vanadium redox flow battery for years, has developed an electrochemical process which allows to regenerate the electrolyte. This process requires the use of a special reactor which, from a design point of view, is similar to the cell of a VRFB. In one half cell of this reactor, a special electrode, a dimensional stable anode, is used to promote the formation of oxygen in order to facilitate the reduction of the vanadium ions in the other half cell, which is important to rebalance the electrolyte.

The goal of this thesis is to run experiments to characterize the new material used, to find a suitable end-point criterion for the recovering process and to calculate the cost of it. The work is organized in three chapters: in the first a comparison between different kind of energy technologies is reported and a detailed description of the vanadium redox flow battery is provided; in the second experimental results for the characterization of the dimensional stable anode are described and discussed and a mathematical model is developed in order to provide an end-point criterion of the recovery process; in the third chapter an economic analysis shows how to calculate the costs both for the vanadium redox flow batteries and the regeneration process by using also a numerical example.

Chapter 1

Vanadium Redox Flow Batteries

In this chapter are provided informations related to different energy storage technologies with a particular attention about the vanadium redox flow battery. Their working principles and their components are below explained.

1.1 Energy Storage Technologies

The rapid development of industrial societies in the last two hundred years was based on the huge reserves of low-cost fossil energy. Resources formed over millions of years have been burned in a relatively short time, with a deep environmental impact. The electrical energy production and consumption are growing significantly as a result of the strong electrical penetration in lots of everyday life activities and of the rapid increase of the world population. Nowadays, electric energy demand exceeds 20 x 10^3 TWh/year and is growing at the rate of 3% per year. Electrical energy is mainly produced through fossil fuel (approx. 2/3 of the total), nuclear and hydroelectric power plants [1,2]. Therefore, even though the fossil fuel represents the main source of energy for all the industrialized countries, the increasing attention to environmental problems have led to their gradual replacement with environmentally-friendly renewable sources. The latter, except for hydropower, currently provide 4% of electricity production mainly from wind and solar energy, but their penetration is estimated to grow by more than 25% by 2030 [3].

Unlike conventional power plants, wind, solar and other renewable sources are intermittent because they generate electrical power according to the time and climatic availability of the resources. The integration of renewable energy sources with the electric grid requires a lot of attention. Indeed, recent studies have suggested that the grid can become unstable if the power from these sources exceeds 20% of the whole generated power without adequate compensating measures, namely energy storage [4,5]. These issues led to combine the energy generation from renewable sources with energy storage system capable of storing production surplus during some periods and of delivering it when requested. Economically convenient and technically competitive storage solutions must ensure not only response time, storage capacity and grid need, but must also show a long lifetime and be able to withstand a large number of charge/discharge cycles [6,7]. The solutions in this field are a lot and they cover a wide range of possibilities.

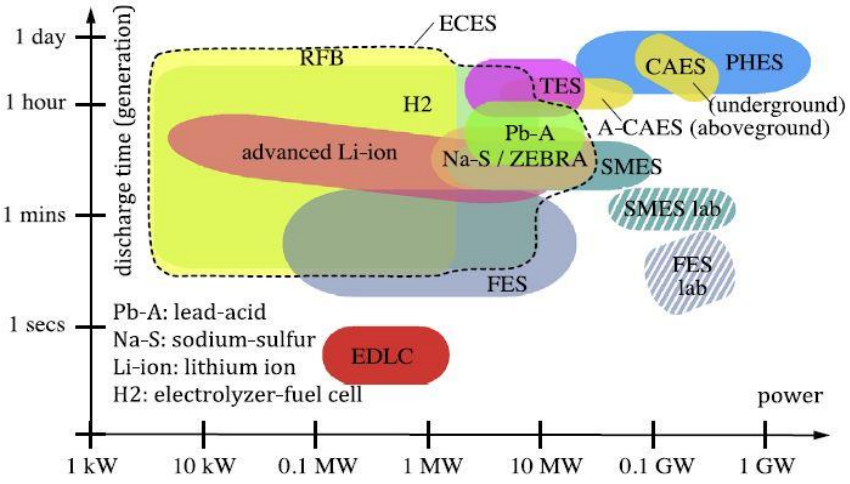

Figure 1.1: *Power-duration diagram of energy storage system: PHES (Pumped Hydro Energy Storage technology), CAES (Compressed Air Energy Storage), TES(Thermal Energy Storage), SMES (Superconducting Magnetic Energy Storage), EDLC (Electric Double Layer Capacitor), FES (Flywheel Energy Storage), ECES (Electro Chemical Energy Storage) [8].*

The diagram in Fig. 1.1 shows where the possible technologies for electrical energy storage are organized according to the discharge time at rated power versus power rating. The diagram is divided into three zones: Power Quality zone in the bottom left corner, characterized mostly by low discharge time and low power; Energy Management zone in the top right corner, for high discharge time and power; finally, in the middle there is the intermediate UPS (uninterruptable power supply) and Bridging Power zone. Every storage technology is characterized in terms of power and energy capacity, response time, capacity loss rate, efficiency, scalability, environmental impact and capital costs, as showed in Tab. 1.1 and in Tab. 1.2. The mostly used system nowadays for energy management is the Pumped Hydro Energy Storage technology (PHES) in which water is pumped up the dams when there is an excess in energy production. Power and energy that can be stored are high and the efficiency of the process can achieve high values. The water reservoir can be stores on a time scale that can be of the order of days or week. On the other hand, this technology can't be decentralized and it needs very particular geographic configuration so that it can't be placed everywhere. Moreover, its response is slow, making it not suitable in the case of sudden request of power. Other technologies in this field but with a lower use are the Compressed Air Energy Storage (CAES) and the Thermal Energy Storage (TES), which are suitable for long time scale (hours) grid energy storage [8].

Table 1.1: *Best performance and typical figures of main energy storage system.*

Technology	Top power [MW]	Top energy [MW h]	Energy density [W h/kg]	Discharge time	Response time	Round-trip efficiency	Cycle life $\times 10^3$	Capital cost [k$/kW]	Capital cost [$/kW h]	Capital cost [$/MW h/cycles]
PHES	3000	10^4	0.3	10^1 h	min	70–85%	20	0.4–5.6	10–350	0.5–3
CAES:										
Underground	300	10^3	10–30	10^0–10^1 h	min	60–	30	1.7	130–550	4–18
Aboveground	50	10^2	–	10^1 h	min	75%	> 10	2.2	430	43
TES	20	10^1	70	h	min	–	10	–	5,000	500
FES:										
Commercial	20	5	11–30	min	ms	85%	10^1–10^2	2.3	2,400	25–200
Lab	400	1	1.6	s	ms	–	–	–	–	–
SMES:										
Under development	100	10^1–10^3	–	min	ms	90–95%	10	2	> 10,000	1000
Lab	400	10	1.2	s	ms	–	–	–	–	–
EDLC	100	10^{-2}	10–30	s	ms	95%	500	–	4,600	10
ECES:										
Advanced lead-acid	10–40	10^0–10^1	25–50	10^0 h	ms	75–85%	3	4.6	130	150
Sodium-sulfur	34	10^1	150–120	10^0 h	s	85–90%	4.3–6	3.5	550	90–130
Sodium-nickel-chlorine[a]	1	6	95–120	10^0 h	s	85%	3–4	3.5	650	150–200
Lithium-ion	16	20	100–200	10^0 h	ms	95%	4–8	3–4	600	150–200
Electrolyzer/fuel cells	1	> 10	800–1300	> 10^0 h	ms	35–45%	50	17	> 10,000	200
Redox flow battery	2–100	6–120	10–50	10^0–10^1 h	ms	85%	> > 13	3.2	900	< < 70

–Means not applicable or unknown.

[a] Data courtesy of FIAMM S.p.A.—Zebra-Sonick (Italy).

The Superconducting Magnetic Energy Storage (SMES), the Electric Double Layer Capacitor (EDLC) and the Flywheel Energy Storage (FES) can operate at low and middle power and provide very fast response time, but are effective on the s-min timescale duration and are very expensive at the present [8]. A more fitted technology that can be better coupled with renewable energy storages is represented by the Electro Chemical Energy Storage (ECES) system.

Table 1.2: *Design and operating features of main energy storage systems.*

Technology	Scalability	Flexibility	W–W h Independency	Environmental impact	Safeness issue
PHES	Good	Low	Yes	High	High
CAES:					
Underground	Low	Low	Yes	High	High
Aboveground	Low	Low	Yes	Low	High
TES	Low	Low	Yes	Mild	Mild
FES:					
Commercial	High	Good	Yes	Low	Mild
Lab	Low	Low	Yes	Low	Mild
SMES:					
Under development	Good	Low	No	Low	Low
Lab	Good	Low	No	Low	Low
EDLC	Low	Low	No	Low	Mild
ECES:					
Advanced lead-acid	Good	Good	No	Low	Low
Sodium-sulfur	Good	Good	No	Low	Mild
Sodium-nickel-chlorine[a]	Good	Good	No	Low	Mild
Lithium-ion	High	Good	No	Low	Low
Electrolyzer/fuel cells	High	High	Yes	Low	Mild
Redox flow battery	High	High	Yes	Low	Low

[a] Data courtesy of FIAMM S.p.A.—Zebra-Sonick (Italy).

They can cover a wide area of applications, due to their site versatility and modularity that allows wide scalability, ease of operation and static structure [9,10].

A specific feature of ECESs is that, in most of them, deep discharges strongly affect the battery life and consequently producers specify a depth of discharge (DOD) less the 100%, at which nominal cell lifespan is referred. Lifespan is the number of cycles for which the cell capacity (i.e. the deliverable charge) does not fall below a given fraction (e.g. 60%) of the nominal capacity (expressed in Ah). In practise, only a part of the energy stored in most ECES device is usable and it is destined to decrease over time [8].

As part of this category there are Li- or Na-based batteries, Pb-acid batteries, fuel cell or H_2 based technologies and redox flow batteries (RFBs). The latter is a kind of technology which in the last years has risen a particular interest out of the scientific community for its promising features. These batteries could be used at medium-high level of storage and mostly for load levelling or power quality control as far as a support to renewable energy source [9].

1.2 Redox flow battery

Redox flow batteries may be classified into three groups according to the phases of the electroactive species presented in the system namely, a) all liquid phases, where chemical energy is stored in the electrolyte, b) all solid phases, where chemical energy is stored in an active material on the electrode plates and c) hybrid redox flow batteries [11].

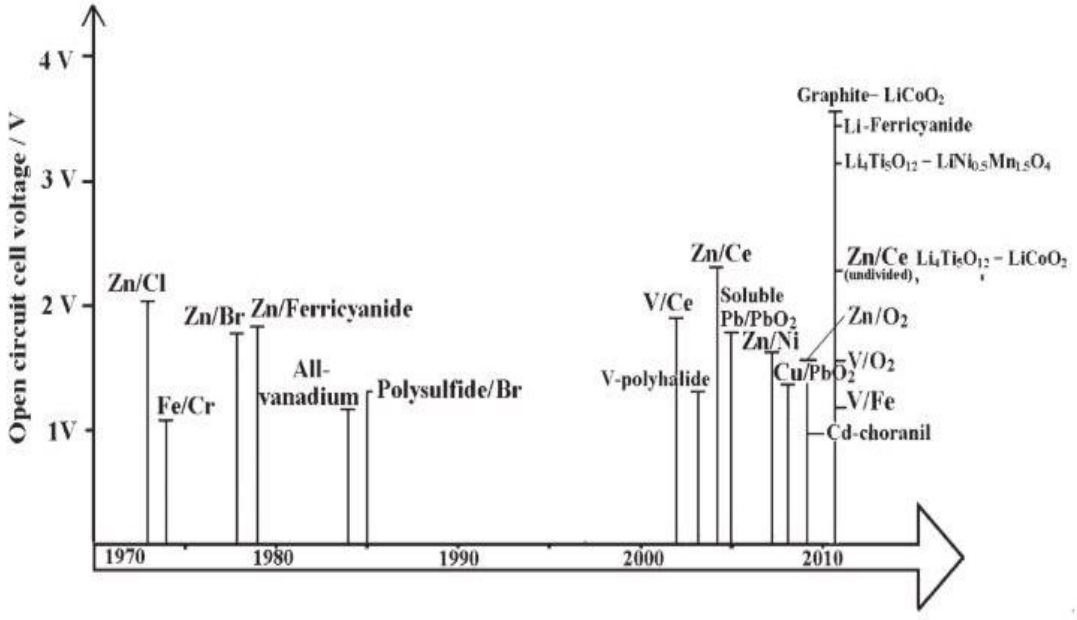

Figure 1.2: *Timeline of the development of redox flow batteries over the past 40 years [11].*

In the first group both redox couples have reactants/products dissolved in the liquid electrolyte and in the second group both redox couples involve solid species during the charge process, whilst hybrid RFBs have redox couples which involve solid or gaseous species at one half-cell.

Among the years, a lot of redox systems were studied, as show in Fig.1.2, but in this work only the first group of RFBs are considered, in particular all vanadium liquid phase.

A typical RFB is mainly composed by four parts, as represented in Fig. 1.3:

1. Two tanks where the electrolyte is stored;
2. An electrochemical cell divided in two sides by an ion exchange membrane;
3. Two pumps to move the electrolyte inside and outside the cell;
4. Power electronics for electricity conversion.

During the charge in one half-cell, precisely at the cathode, an oxidation occurs providing electrons and ions: the first are forced to take an external circuit to go in the opposite half-cell, the anode, where the electron is used to reduce the other metal ions presented in the electrolyte; the ions instead migrates through the membrane in order to satisfy the electrical balance between in the solution. The kind of ions which migrate, positive or negative, depends on the type of membrane used: anionic or cationic. During the discharge, the opposite reactions take place: at the anode the oxidation and at the cathode the reduction. Therefore, electrons and protons move in the opposite direction too. Compared to other electrochemical storage technologies, in RFBs power conversion is separated from energy storage, therefore power and energy are independent from each other [11].

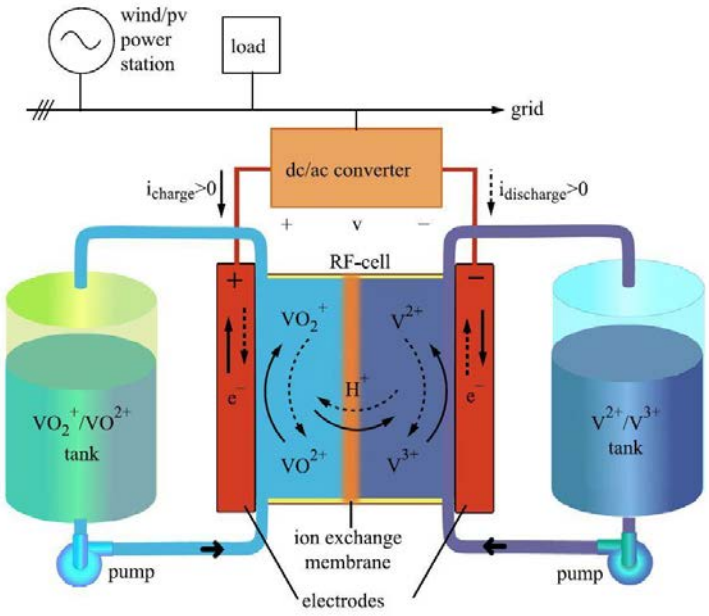

Figure 1.3: *Process flow diagram of an RFB energy system: the electrochemical cell and the electrolyte tanks are separated.*

In fact, power depends on the size of the active area where the electrolyte reacts and on the number of the cells in the stack, while the energy depends on the concentration of the electrolytic solutions and on the size of the tanks which contain them. This feature allows for virtually unlimited capacity simply by using larger storage tanks and unlimited power simply by connecting more cells in series. Practically speaking, energy of present design spans from 10^2 to 10^7 Wh, a range that exceeds most of the other ECES for at least one order of magnitude (See Tab. 1.1). Another advantage is that the RFB reactions are completely reversible, enabling the same cell to operate as converter of electricity into chemical energy and vice-versa. Moreover, RFBs operate by changing the metal ion valence without consuming ion metals, thereby allowing for long cycle service life; they can be discharged completely or overloaded for short periods of time: that means that the battery can be totally discharged without affecting their performance. Self-discharge doesn't occur because the two electrolytes are stored in different tanks and cells can be left completely discharged for long periods with no ill effects. Finally, RFBs are capable of rapid response that allows them to span from power quality to energy management services, they present high values of efficiency, they are easy to scale up or down and their environmental footprint is very low [8].

The mainly disadvantages are: first, the power density and energy density of RFBs are low compared to other technologies, making them unsuitable for mobile applications at present; second, since electrolytes are conductive, they are prone to shunt currents which produce additional losses and affect electric efficiency and third some ions may cross the membrane and diffuse into the opposite half-cell due to concentration gradients (cross-over effect) [8, 11].

1.3 Vanadium redox flow battery

1.3.1 Main features

Among the RFBs, the most promising are the all-Vanadium or VRFBs. The reasons are different [11,12]:

1. By using the same electrolyte in both half-cell, the cross-contamination is lowered significantly;
2. It works at room temperature and the thermal control can be simply performed by periodic recirculation of electrolyte solution in the stack;
3. There is an extremely low rate of gas evolution during the charge rates associated with the rapid charging cycles;

4. It does not require a catalyst for each electrode reaction because of the fast kinetics of the vanadium redox couples.

Of course, there are also some disadvantages by using Vanadium as electrolyte, the main ones are the following four [12]:

1. They have low values of power and energy density: nowadays energy density float around 10-35 kW/kg which is around ten times lower of a Li-based battery. The energy density in a VRFB depends on the concentration of vanadium species but there is a limited vanadium concentration in the electrolyte due to the precipitation of solid vanadium compounds;
2. It presents side reactions which may cause loss of capacity over extended cycling. In particular V(II) is sensitive to oxygen and it should be kept in a protected atmosphere to avoid its oxidation.
3. The highly oxidizing nature of V^{5+} can cause degradation of the ion exchange membrane and the electrode material.
4. The disposal of Vanadium at the end of its life cycle is not straightforward.

1.3.2 Electrolyte and reactions

Vanadium is a rare transition metal mostly employed for special steel production. It is present in several minerals and can be rarely found pure in nature. It's produced mostly as a by-product in steel production from steel smelter slag or from the flue dust of heavy oil or even from uranium mining. All its compounds are classified as toxic and the United States National Institute for Occupational Safety and Health (NIOSH), classified some of them as immediately dangerous to life and health because they are likely to cause permanent health problems or death. Vanadium based electrolytes for VRFB are made by $VOSO_4$ in H_2SO_4 and for this reason they are quite corrosive so that metal parts in the battery equipment must be avoided. That means pipes, pumps and tanks must be produced using plastic or compound materials. An example is PVC (Polyvinyl Chloride), which is cheap and largely available on the market. The metal ions in the electrolyte reflect the four oxidation states of Vanadium: V(II), V(III), V(IV) (in the form of VO^{+2}) and V(V) (in the form of VO_2^{+}) [12].

Table 1.3: *Electrochemical reactions which occur in VRFB during charge and discharge.*

Charge/Discharge	Electrode	Reactions	Standard potential
Charge	Positive	$VO_2^+ + 2H^+ + e^- \rightleftarrows VO^{2+} + H_2O$	E_C^0 = -1.004 V
	Negative	$V^{3+} + e^- \rightleftarrows V^{2+}$	E_A^0 = 0.225 V
Discharge	Positive	$VO_2^+ + 2H^+ + e^- \rightleftarrows VO^{2+} + H_2O$	E_C^0 = 1.004 V
	Negative	$V^{3+} + e^- \rightleftarrows V^{2+}$	E_A^0 = -0.225 V

The electrochemical reactions during the charge and discharge are described in Tab. 1.3. When the battery is fully charged, there are only V(V) and V(II) ions in the solutions, and, as the battery is discharged, they are converted into V(IV) and V(III). Each of these oxidation states is characterized by a peculiar colour (V(II) purple, V(III) green, V(IV) blue, V(V) yellow) so that colours can give a preliminary information over the State of Charge (SOC) of the battery.
The overall electrochemical reaction is:

$$VO_2^+ + 2H^+ + V^{2+} \leftrightarrow V^{3+} + VO^{2+} + H_2O \quad .$$

The standard potential, or standard open circuit voltage (OCV), is $E^0 = (E_C^0 - E_A^0)_{Discharge}$ = 1.23 V at 25°C. This value can be justified also from a thermodynamics point of view [18]. Even if the energy capacity of the system increases with the concentration of vanadium salts, electrolyte solutions must not overcome their solubility limits in order not to enhance the precipitation. As the solubility varies with the temperature it's important to set some limits in the working range. It has been demonstrated and long investigated since the 1980s, that if the working conditions floats between +10 to +50 °C precipitation is avoided with molarity of vanadium as high as 2.5 M [12].
A Vanadium electrolyte solution of 50:50% mole fraction of V^{3+} and V^{4+} with a total vanadium composition of 1.6M in 2M of sulfuric acid and in 0.05 M of phosphoric acid was used as electrolyte for all the experiments reported in this study.

1.3.3 General structure of a single cell

A general structure of a single VRFB cell is shown in Fig. 1.4. The cell is divided in two halves through an ionic exchange membrane. Each half-cell is mainly composed by a cell frame, a current collector, a flow frame, a bipolar plate and an electrode. The union between the membrane, the electrode and the bipolar plate is called MEA (membrane electrode assembly). The MEA is the core of the battery and it is where the most improvement for battery efficiency can be done [8].

1.3.3.1 Electrodes

The electrodes are the sites where electrochemical reactions occur, but they don't take part in them directly. They are used only to provide and to accept the electrons. To obtain high energy efficiency they must ensure a high electrochemical activity and reversibility for the redox couples, ensure good conductivity to prevent ohmic losses and have a stable 3D structure with a high specific area, providing narrow channels for the electrolytes to wet them. Moreover, they must be chemically, mechanically and electrochemically stable but with a reasonable cost to meet the large-scale production. Typically, Carbon-based materials are chosen for V-RFBs. Different prototypes or commercial products show different choices between the available technologies depending on costs versus performance. Carbon felts, adequately carved graphite plates, graphite felts, carbon paper or nano-scaled carbon tubes are some of the technologies that can be employed. Their performances can be modified by adding electrocatalysts species or according to the management of the electrolytes flux or the shape of carving in the solid current collectors [12].

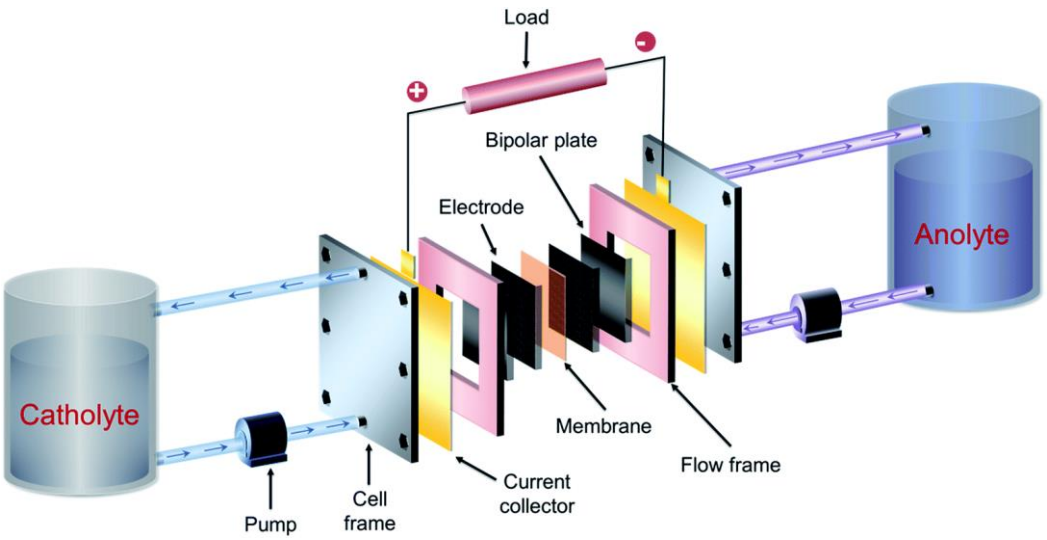

Figure 1.4: *General structure for a single VRFB cell.*

1.3.3.2 Membrane

The membrane separator is a key component of VFB, playing the role of isolating electrolytes (vanadium ions) while still transferring ions (protons, SO_4^{2-}) to complete the circuit. The ideal membranes should possess high ion selectivity, ion conductivity, and good chemical and mechanical stability. The membranes traditionally used in VFB are perfluorinated sulfonic acid polymers such as Dupont's Nafion. Although they show both high proton conductivity and chemical stability, the extremely high cost and low ion selectivity of these membranes (high vanadium crossover) have limited their further commercialization. Hence, alternative ion exchange membrane (IEM) materials are being sought. Quite recently, different kinds of IEMs including anion or cation exchange and even blend membranes were investigated in VFB applications. The current research is mainly focused on two critical issues of VFB membrane separators. One is mainly devoted to increasing membrane selectivity, while the other important task will be focused on improving membrane stability. The selectivity of membranes in the VFB is largely determined by the membrane morphology. Two regions normally coexist in traditional IEMs, a hydrophilic and a hydrophobic one. The distribution of these two regions will largely affect membrane properties like ion selectivity, ion conductivity, and mechanical and chemical stability. Various factors could affect the microphase-separated morphology of IEMs, among which, the nature of polymer chains could be one of the most important ones [12].

1.3.4 Construction and design of the Cell Stack

In real applications, the batteries are assembled from several single cells to form a battery stack. Electrodes are situated on either side of a bipolar plate, which separates each cell from the next one. The assembly of a cell stack is a straightforward mechanical process. Electrodes, membranes, and bipolar plates are manufactured to form a stack. Large steel end plates provide mechanical integrity. The cell size can be determined from the desired power rate, but in practice, cell size is driven by many other factors, such as mechanical strength, thermal stability, the dimension of the components and shunt current. The construction of a cell stack is shown in Fig. 1.5. Most cell stacks are constructed in a Parallel-Feed design, as it is shown in Fig. 1.4 where all the single cells operate with the same inlet and the electrolyte is then distributed to all the cells via an internal manifold system. In this way all the cells work with the same concentration of active species and a similar volumetric flow rate. In order to avoid gas bubbles to stays in the active area, a lower outlet with respect to the inlet is suggested. The main drawback is represented by the formation of shunt currents inside the electrolytes which lower the overall efficiency and can give thermal instability.

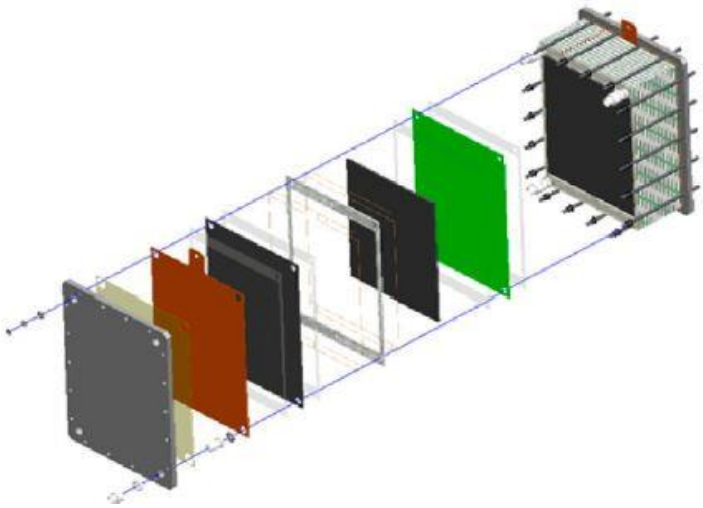

Figure 1.5: *The assembly of a cell stack [12].*

Anyway, this is the most convenient configuration for both small or medium-size RFBs [12].
An alternative is the Series-Feed design where the cells are, in this case, arranged in cascade so that the electrolytes flow successively through each of them. That leads to a different concentration of reactants in every cell and to a non-uniform distribution of flow. This method results in a higher pressure drop as well. In theory shunt currents should be avoided. This mode needs for a model which keeps under control the progressive reactants consumption in order to ensure that the final cell in the cascade is not underfed [12].

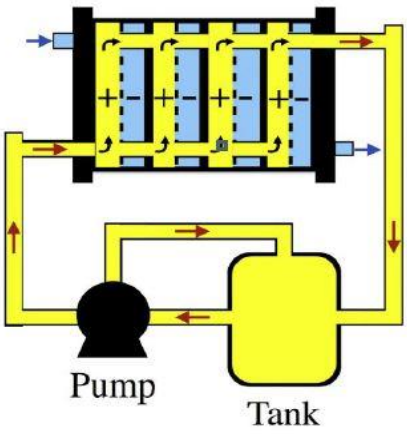

Figure 1.6: *Parallel Feeding for a VRFB. Only the circulation of one of the two electrolytes is shown.*

Chapter 2

Electrolyte Regeneration in Vanadium Redox Flow Batteries

In this chapter the electrolyte regeneration is described. In particular the experimental procedure adopted and the mathematical model developed.

2.1 Electrolyte imbalance: causes and monitoring

Vanadium salts dissolved in sulfuric acid are used for energy storage in all-vanadium redox flow battery. As described in chapter §1, during battery discharge vanadium species undergo redox reactions of V^{5+} to V^{4+} in the positive half-cell, and V^{2+} to V^{3+} in the negative half-cell. A commercially available mixture of V^{+3} and V^{+4} species in a 50:50% mole ratio (referred to as $V^{3.5+}$ electrolyte) is often used as a starting electrolyte for VRFBs and needs to be charged to form V^{3+} in the negative tank and V^{4+} in the positive tank for further battery operation.

During long-term performance the VRFB electrolyte is reported to become unbalanced. Imbalance implies an inequality in the amount of oxidized and reduced species in the two tanks and it is usually caused either by vanadium cross-over through the membrane or by side reactions such as hydrogen evolution in the anolyte or air oxidation of V^{2+} ions in the negative side. It results in capacity losses and 100% state of charge (SoC) can then be achieved only in one half-cell.

While any capacity loss caused by a crossover effect can be readily corrected by simple periodic electrolyte remixing that rebalances the electrolyte compositions and liquid levels in each reservoir, capacity losses by side reactions can only be corrected by chemical or electrochemical rebalancing of the oxidation state of the two half-cell electrolytes.

Suitable state of charge monitoring is therefore needed to detect any imbalances in the individual electrolyte oxidation states, so that appropriate correction procedures can be applied to restore any loss of capacity. Traditionally, open circuit cells are used to monitor the state of charge of a cell by using the Nernst Equation. Although the open circuit cell voltage (OCV) can be used as indication of the overall state of charge, this will only be accurate if the system is balanced. If the electrolyte becomes unbalanced, cell SoC cannot be accurately indicated by the OCV, because the state of charge of the positive half-cell is not the same of the negative one. Ideally therefore, each of the half-cell electrolyte potentials should be monitored so that the SoC of each half-cell electrolyte can be independently monitored [13].

Theoretically an inert indicator electrode could be utilized in each half-cell, however, in a large-scale redox flow cell system the use of such an electrode would be impractical since solution potential measurement also requires a stable reference electrode potential. Reference electrode however are inherently unreliable due to a large number of interferences that can lead to drifts in the measured potential. Furthermore, the solution potential changes only slightly over a wide range of states-of-charge so that sensitivity is poor. Other alternatives methods of SoC monitoring have thus been investigated, such as conductivity measurements or absorption measurements based on spectrophotometric principles. The first uses the linear variation in electrolyte conductivity with SoC, while the second uses light absorption to take advantage of the solution colour changes during charging and discharging of the electrolyte. in this work the latter was used and it will be explained in more detail in next paragraphs [13].

2.2 Solutions for the imbalance

Generally, there are several approaches to restore the V^{3+}: V^{4+} ratio:

- Adding V^{3+} salt to compensate the decrease in its concentration: this is, however expensive (V^{3+} is available mainly as vanadium(III) oxide) [15].
- Reducing an excess of V^{4+} chemically: for example, introducing foreign species into the electrolyte, but then the electrolyte would be contaminated by the products of this reaction [15].
- Remixing the electrolyte: however, this method requires the pre-charging of the electrolyte before restarting the battery operation, making it non efficient in terms of energy [14].
- Partial reduction of V^{5+} via the addition of organic compounds to the positive tank, even though this method leads to a volumetric imbalance between the two tanks and might be difficult to realise in large scale battery system [14].
- Electrochemical reduction of the electrolyte: this can be performed in an anodic half-cell coupled with an oxygen evolution reaction from sulfuric acid solution in the cathodic half-cell. Here special care should be taken in the catalysis of the oxygen evolution reaction. Furthermore, it is not always straightforward to set the end point of the electrolysis to achieve predefined V^{3+}: V^{4+} ratio and it is may be not efficient in terms of energy too [15].

In this study an electroreduction process was set up and analysed as shown in the following chapters.

2.3 Electroreduction regeneration process

As introduced in the paragraph §2.1 of this chapter, the electrolyte unbalancing may appear after long-time operational discharging-charging cycles. In order to better understand where and how a regeneration process has to be implemented, it is better analysing more in detail what happens inside of the flow battery during its operation. The starting point is a standard electrolyte with a fixed concentration of $V^{3.5+}$ for both tanks: positive and negative (in different words: catholyte and anolyte). When the anolyte and the catholyte are charged, in the negative side there should be 100% of V^{2+} and in the negative side 100% of V^{5+}. But after long-time operation this condition may not be true anymore: side reactions lead to a change in ions composition. In particular the oxidation of V^{2+} through the reaction (2.1):

$$V^{2+} + \tfrac{1}{2}O_2 + 2H^+ \rightleftarrows V^{3+} + H_2O \qquad (2.1)$$

For this reason, some of the V^{2+} ions become V^{3+} and consequently the SoC in the negative side decreases, leading to an imbalance between the catholyte and the anolyte, as represented in Fig. 2.1.

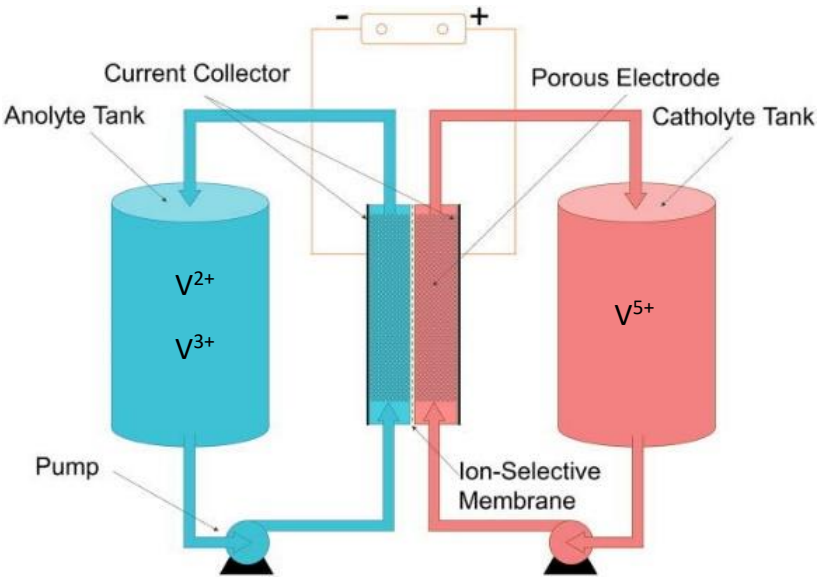

Figure 2.1: *Effect of side reactions on the negative tank of VRFB: due to the oxidation of V^{2+} in the anolyte tank some V^{+3} ions are produced and a SoC = 100% can be reached only in the catholyte tank leading to an imbalance between the two sides.*

Table 2.1: *Reactions which take place in the electrochemical regeneration reactor.*

Charge/Discharge	Electrode	Reactions	Standard potential
Charge	Positive	$VO_2^+ + 2H^+ + e^- \rightleftarrows VO^{2+} + H_2O$	E_C^0 = -1.004 V
	Negative	$2H_2O \rightleftarrows O_2 + 4H^+ + 4e^-$	E_A^0 = -1.23 V

Therefore, in order to overcome this problem, the V^{3+} in the anolyte has to be reduced again to V^{2+} and the electron needed for this reaction can be provided by the oxidation of V^{4+} to V^{+3} that takes place in the catholyte tank (see Tab 1.3). Since the catholyte tank, at 100% of SoC, doesn't have V^{4+} ions to be oxidized, these have to be produced through an electrochemical process, which is presented in Fig. 2.2. The idea is to reduce part of the V^{5+} stored in the positive tank, by using an electrochemical reactor. In this way, V^{4+} can be produced and can be used then to provide the electrons necessary to reduce V^{3+} into V^{2+} ions inside of the battery, bringing the SoC of the anolyte tank up to 100%. The electrochemical reactor is a cell which has the same structure of the VRFB one: it is divided in two half-cells from an ionic exchange membrane where two different reaction take place: at the positive pole V^{5+} is reduced to V^{4+} and at the negative pole water is oxidized producing oxygen, as described in Tab. 2.1.

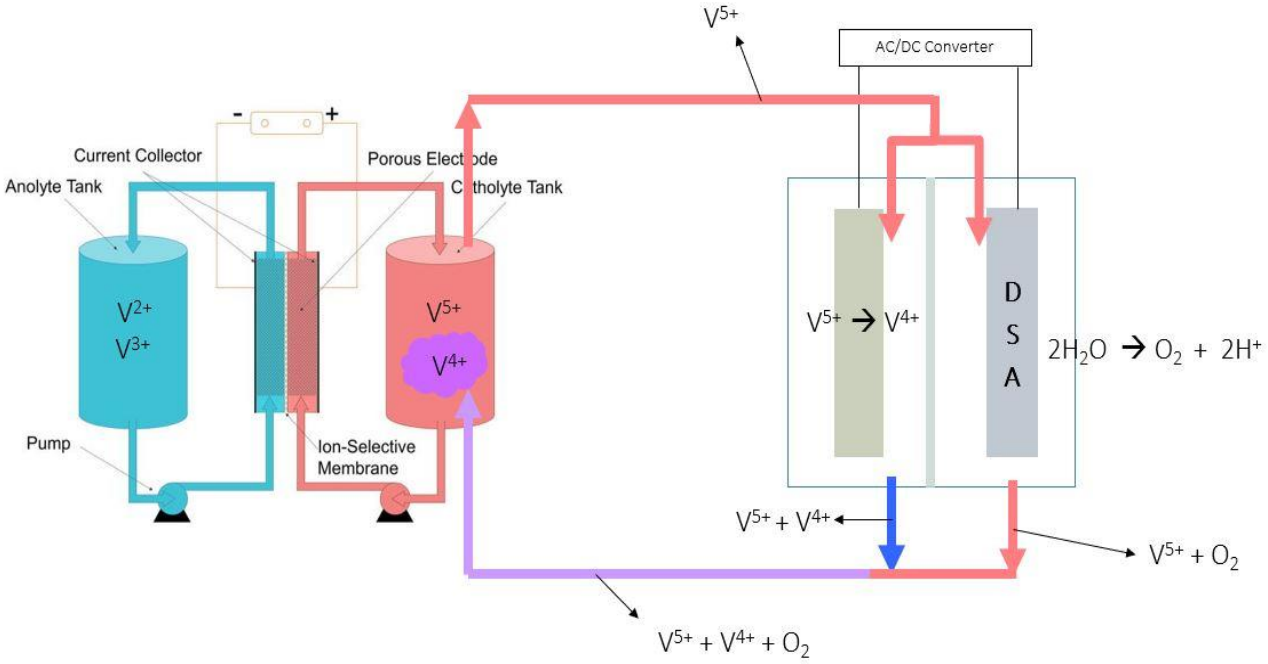

Figure 2.2: *Scheme of the electrochemical regeneration process.*

If for the positive pole a normal carbon felt electrode is used, for the negative pole the electrode is different. A dimensional stable anode (DSA), made by titanium and coated with catalyst, is needed in order to promote the oxygen formation,

2.4 Regeneration reactor performance

In this paragraph a qualitative and quantitative description of the performance of the regeneration reactor are given. Furthermore, the experimental setup adopted will be described and then the final results will be discussed. Origin® was the software used to plot the results.

2.4.1 Materials

The setup of the regeneration reactor was similar to that of the regular VRFB cells that were used in this work: the cell is divided in two halves through an anionic exchange membrane (Fumasep, FAP-450, FuMa-Tech GmbH, Germany) and each half-cell was composed by: a cell frame, a current collector, a flow frame, a FU 4369 graphite bipolar plate (Schunk Kohlenstofftechnik GmbH, Germany) and an electrode with an area of 40 cm^2. This latter represents the only difference between the VRFB cell and the regeneration reactor. in the positive side of the cell, the GFA6 graphite felt (SGL Group, Germany) is substituted with a dimensional stable anode (DSA), as shown in Fig. 2.3. The DSA electrode used in these experiments was produced by DE NORA S.p.A (Milano, Italy) and it is made by titanium and iridium oxide as catalyst. Its particular shape, as shown in Fig. 2.4, helps the oxygen, which is produced on the surface of the catalyst, to pass through the electrode and to come out of the cell [16].

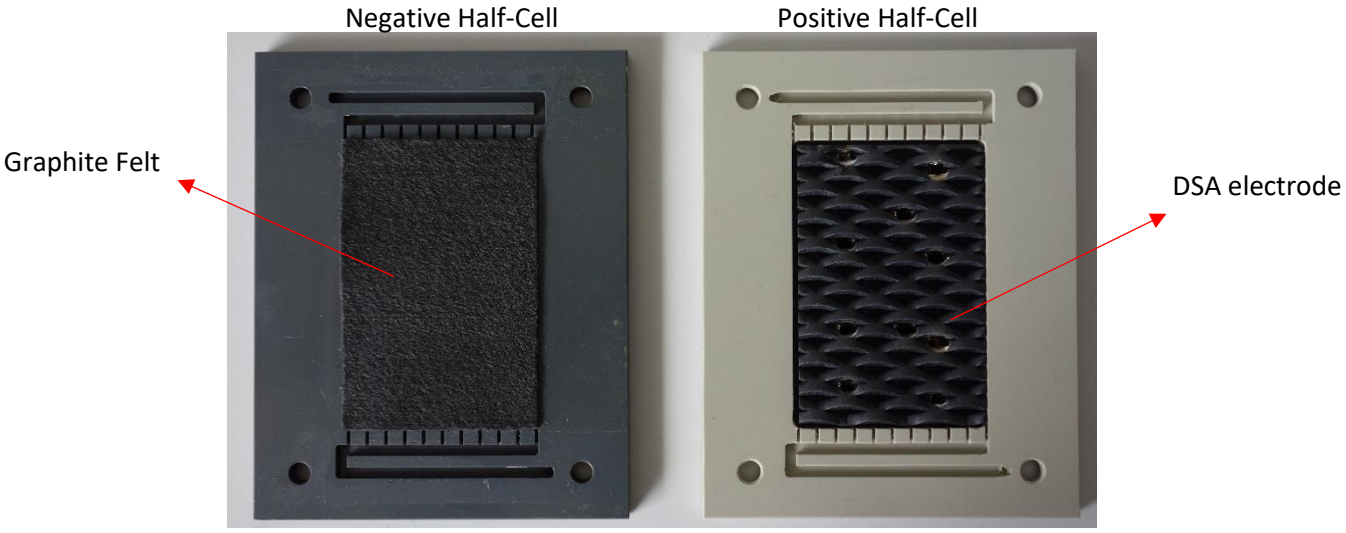

Figure 2.3: *Particulars of flow frame and electrode for the negative half cell (left) and positive half cell (right)*

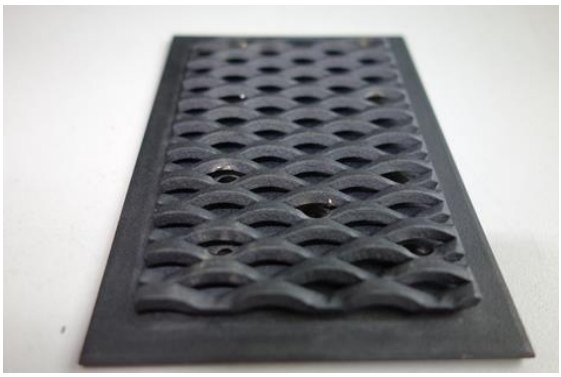

Figure 2.4: *DSA electrode used for the positive half-cell.*

2.4.2 Experimental procedure

In order to evaluate the performance, the voltage-current behaviour (polarization curve) of the regeneration reactor was investigated by carrying out six experiments, as shown in Tab. 2.2. In the first three, volumetric flowrates of electrolyte were varied in order to see how the performance is influenced by the flowrate. In the other three, different temperatures were used. The minimum and maximum value chosen for the flowrates corresponds to the inner and upper limit of the pump; for the temperature, instead, the minimum value corresponds to the room temperature and the maximum one was chosen in order to avoid Vanadium salts precipitation in the electrolyte, which may damage the cell itself. For the temperature dependent experiments, the lowest value of electrolyte flowrate was chosen because, as will be shown later, the cell resistance in this condition is higher and therefore the goal was to evaluate a performance improving by changing the temperature.

Table 2.2: *Number of experiments carried out with the values of flowrates (both as absolute values or respect to the stochiometric flowrate) and temperature for each of one.*

Experiment	Flowrate [mL/min]	Flowrate[1] [-]	Temperature [°C]
1	45	105	20
2	90	238	20
3	160	424	20
4	45	105	25
5	45	105	30
6	45	105	35

[1] Electrolyte flowrate calculated respect to the stoichiometric one, which is $1x10^{-5}$ mols/s.

The procedure adopted was the same for all of them:

- Feeding the regeneration reactor with a fixed volumetric flow rate of V^{5+};
- Charging the electrolyte with a constant current of 1 A for a time equal to 30 seconds. Then increasing the value of the current of 200 mA every 30 seconds until a value of 2.4 A is reached. The charge cell tests were performed using a Basytec battery tester (Basytec GmbH, Asselfingen, Germany) in a galvanostatic mode.

The V^{5+} pure electrolyte was produced by pre-charging a vanadium solution of 50:50% mole fraction of V^{3+} and V^{4+} with a total vanadium composition of 1.6M in a volume V = 400 mL.

2.4.3 Results

In Fig. 2.5 and Fig. 2.6 the results are presented in terms of polarization curves: the first one shows the behaviour as function of flowrate and the second one as function of temperature. As can be observed, by increasing the flowrate, the resistance of the cell, which is represented by the slope of the curves, decreases. This means that it is better to use high flowrates instead of low ones. The reason is due to the oxygen formation: increasing the flowrate, the molecules of oxygen are able to come out faster from the electrode. This opens up a higher surface area for the electrochemical reactions to take place. Furthermore, higher flowrates reduce the transport limitation inside of the cell. Instead, the temperature dependence is not very clear: probably this is due to the fact that, increasing the temperature, the kinetics also increases and therefore the formation of oxygen is higher. But since the flowrate is the lowest one, the positive effect of the temperature on the kinetics is cancelled by the transport limitations that increase inside the cell.

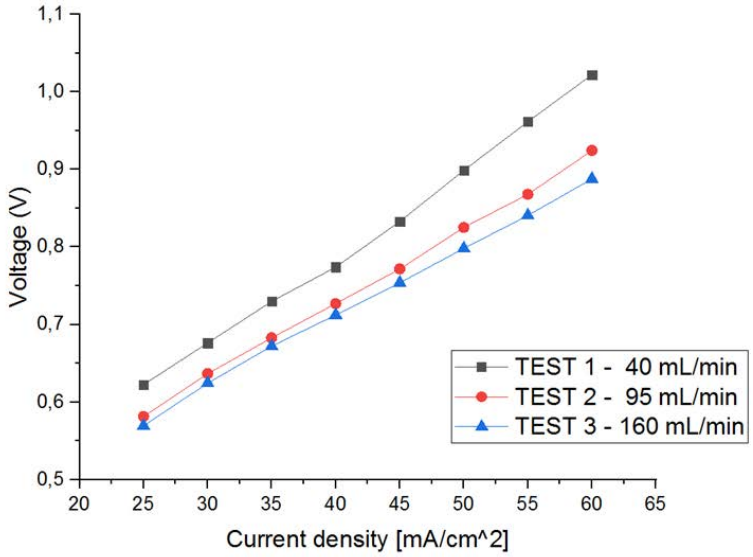

Figure 2.5: *Polarization curves as function of flowrates.*

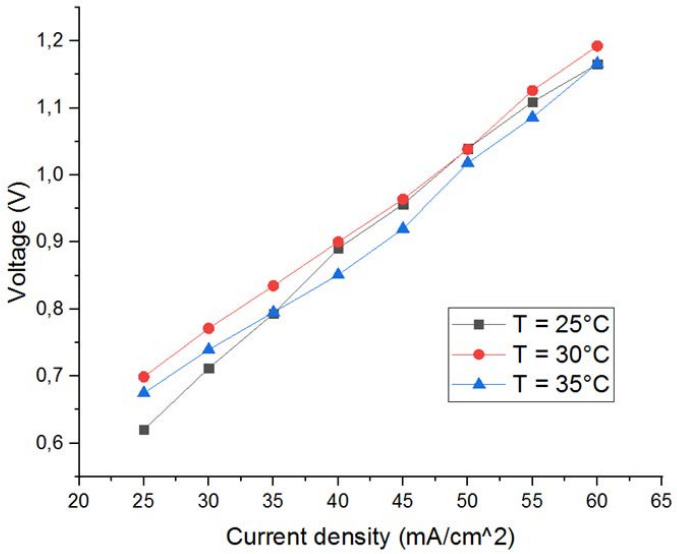

Figure 2.6: *Polarization curves as function of temperature.*

Therefore, higher temperatures are not enough to enhance the performance of the reactor because of the transport limitation and higher flowrates are needed, but then this make the system not more efficient in terms of energy.

Thanks to these experiments it was possible to calculate the coulombic efficiency of the electrochemical reactor. It may be defined like the following:

$$\eta = \frac{Q_P}{Q_u} \ , \tag{2.4}$$

where Q_p is the total charge provided by the power supply for the duration of each experiments (6 minutes) and Q_u is the charge used by the electrochemical reaction to take place and can be calculated with the following equation:

$$Q_u = (N_{V5+}^0 - N_{V5+}^t) * F \quad , \tag{2.5}$$

where N_{V5+}^0 is the number of moles of V^{5+} at the beginning of each experiment, N_{V5+}^t is the number of moles of V^{5+} at the end of each experiments and F is the Faraday constant equal to 96485 $Cmol^{-1}$. In order to calculate the number of moles of V^{5+} used in equation (2.7) it is necessary to measure the composition of the electrolyte before and after each experiment. This can be done through a potenziostatic titration.

Table 2.3: *Parameter and quantities used to calculate the coulombic efficiency.*

Experiment	Volume [mL]	Q_p [C]	N_{V5+}^0 [mol]	N_{V5+}^t [mol]	Q_u [C]	η [%]
1	400	458,78	0,633	0,62204	285,85	62,31
2	400	458,78	0,633	0,61895	366,46	79,88
3	400	458,78	0,633	0,61856	376,53	82,07
4	400	458,78	0,633	0,61967	347,60	75,77
5	400	458,78	0,633	0,61945	353,50	77,05
6	400	458,78	0,633	0,62082	317,55	69,22

As it is shown in Tab 2.3, the coulombic efficiency varies in a range between 62,31 % to 82,07%. Increasing the flowrate has a deep impact on the efficiency: higher flowrates means higher efficiency and this is related to the fact that the resistance in the cell is slower, as already discussed before. The temperature, instead, does not have a clear effect on the efficiency.

2.5 Regeneration process: experiments and modelling

In this chapter, the response of the VRFB cell to a changing in composition due to the regeneration process is analysed: in particular the experimental setup adopted will be described, then a mathematical model will be provided to have a better understanding of the overall process and finally the obtained results will be discussed and compared with the model.

2.5.1 Experimental procedure

The starting point of this experiment is to generate an already unbalanced electrolyte, in order to avoid to wait that an imbalance take places in the cell. Therefore, 32 mL of pure V^{3+} are mixed with 48 mL of pure V^{4+} to obtain a Vanadium electrolyte solution with a mole fraction of 40:60 % V^{3+} to V^{4+}, or an imbalance of 20%. Then, this electrolyte is fed into a VRFB cell with a constant flowrate of 160 ml/min. Through the battery test system, a constant current of 1 A is applied to the two current collectors of the positive and negative side. When the voltage reaches the value of 1,65 V, the electrolyte starts to be charged with a constant voltage of 1,65 V. A UV/Vis Spectrophotometer (HR2000+, Ocean Optics, USA) is used to continuously measure the SoC of the negative side as it is shown in Fig. 2.7 (see App. B for further information). Furthermore, a constant flowrate of nitrogen is fed to the negative tank in order to avoid the air-oxidation of the V^{2+} formed during charging.

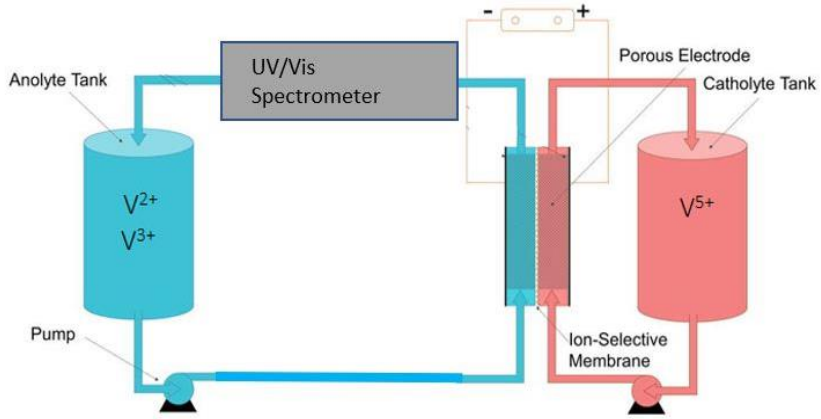

Figure 2.7: *Location of the UV/vis Spectrometer.*

Fig. 2.8 shows the dynamic behaviour of the current, of the potential and of the SoC of the cell. At the beginning the current remains constant because the cell is charging galvanostatically and the potential of the cell increases. Then, when the charging process is switched to potenziostatic mode the current starts to decrease and the potential remains constant. The formation of V^{2+} in the anolyte leads the SoC to increase. as soon as the current reaches a steady state, the SoC becomes constant. At this point, the current is very low and this means that the battery is close to be fully-charged. But, since the initial electrolyte had an imbalance of 20%, only the catholyte is completely charged (100% of SoC), and the anolyte, instead, as shown in right plot of Fig. 2.8, has a SoC equal to 80%. This means that the anolyte is left with 20% of V^{3+} which has to be reduced in order to reach 100% of SoC in the negative tank. Therefore, the regeneration reactor now can be used as presented in Fig. 2.9.

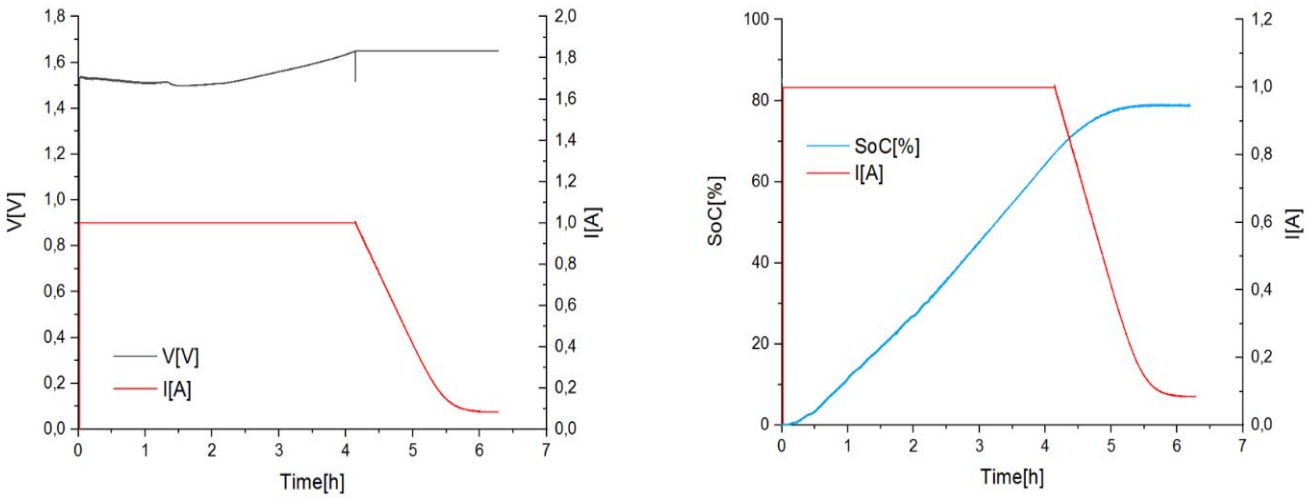

Figure 2.8: *Dynamic behaviour of the potential and of the current (left). Dynamic behaviour of the current together with the SoC of the negative tank.*

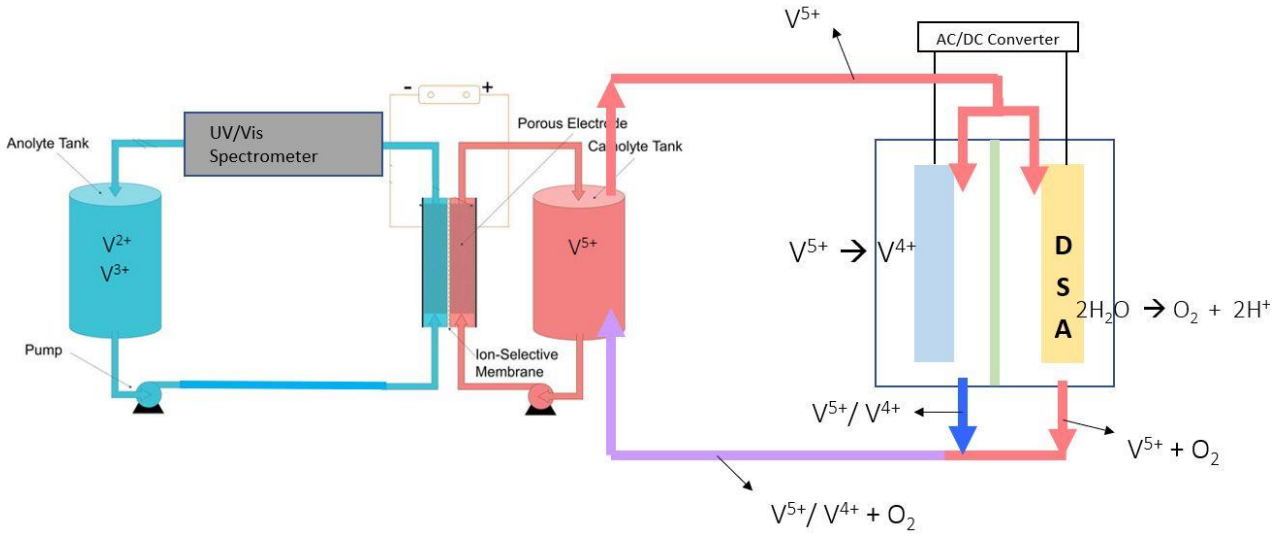

Figure 2.9: *Scheme of the electrochemical regeneration process.*

The DSA reactor is now charged with constant current of 1 A and, as soon as the V^{4+} produced enters into the catholyte tank, the current starts to rise again, as it is shown in Fig. 2.10. This means that the V^{4+} is immediately oxidised to V^{5+} and the V^{3+} is reduced to V^{2+}, as wanted. Indeed, the SoC of the negative side starts to increase as well. By looking at the dynamic behaviour of the current it is possible to observe a maximum point: the physical reason of this behaviour will be given in the next paragraph, where a physical model will be developed. After about two hours and thirty minutes the current in the VRFB cell reaches again a new steady-state. But now, since the regeneration process has never stopped, it is the catholyte not completely charged and the anolyte, as expressed by the blue line in the Fig. 2.10 (right plot), has reached an SoC of around 100%.

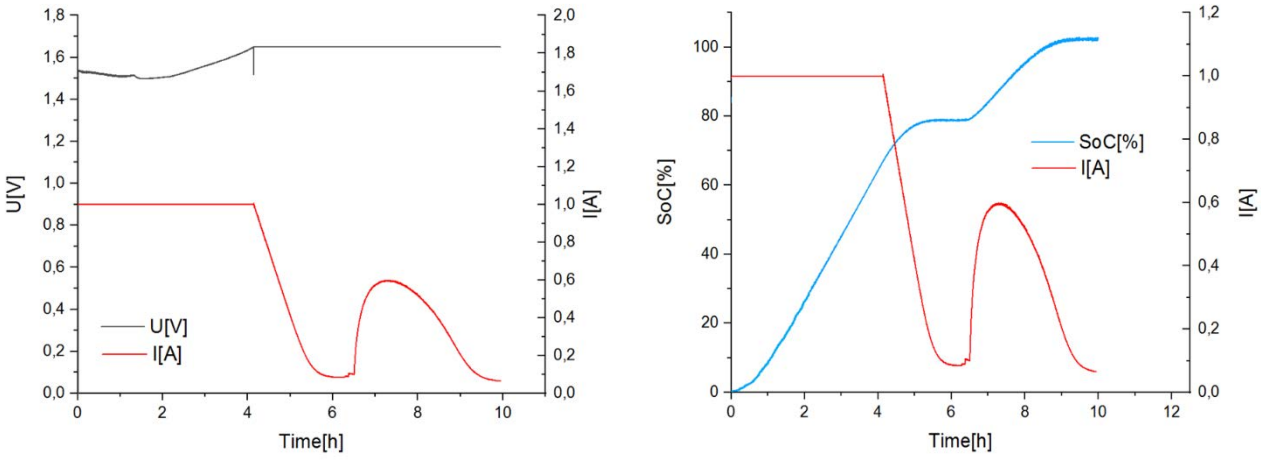

Figure 2.10: *Dynamic behaviour of the potential and of the current (left). Dynamic behaviour of the current together with the SoC of the negative tank (right).*

This means that, the V^{4+} produced by the regeneration reactor is too much in respect to the amount necessary to restore the initial imbalance and now, an 'overshoot' of 20% is obtained. In order to avoid this overshoot, an end point of the regeneration process has to be found.

2.5.2 Mathematical model for the regeneration process

In order to have a better understanding of the dynamic behaviour of the VRFB cell while the regeneration process is activated, a mathematical model has to be developed. This model is based on the mass balance for each vanadium ion considering four different control volumes:

- The regeneration reactor;
- The positive tank;
- The VRFB cell;
- The negative tank.

For each reference volume a dynamic mass balance will be written in respect to V^{5+}, V^{4+}, V^{3+} and V^{2+}.

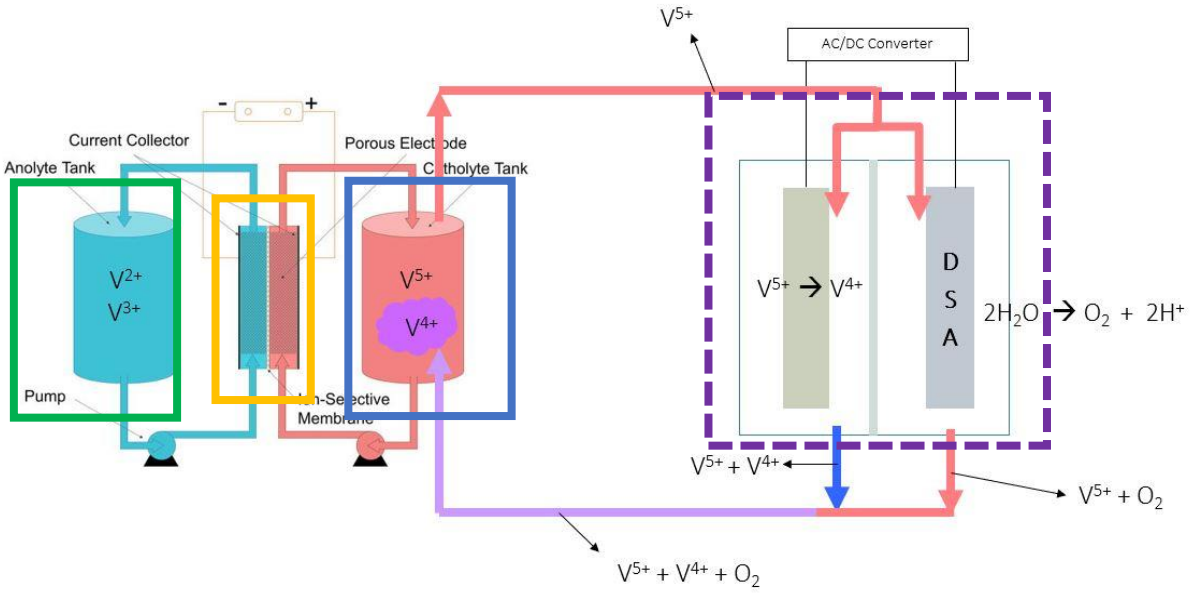

Figure 2.11: *Reference volumes considered for the mass balances: the violet for the regeneration reactor, the green one for the negative tank, the yellow one for the VRFB cell and the blue one for the positive tank.*

2.5.2.1 Regeneration reactor

By considering the reference volume presented in Fig. 2.11, the mass balances for V^{5+} and V^{4+} is expressed by the following equation (where with *i* it is considered a generic ion, which can be V^{+5} or V^{4+}):

$$\frac{dN_i^R}{dt} = \dot{n}_i^{in} - \dot{n}_i^{out} + \dot{n}_i^G \tag{2.6}$$

Where:

- $\frac{dN_i^R}{dt}$ = accumulation term for the generic ion *i* in the reactor ;
- $\dot{n}_i^{in}$ = inlet molar flow rate for the generic ion *i* ;
- $\dot{n}_i^{out}$ = outlet molar flow rate for the generic ion *i* ;
- $\dot{n}_i^G$ = generation terms for the generic ion *i*;
- The generation term is positive for V^{4+} (it is Produced) and negative for V^{5+} (it is Consumed):

$$\dot{n}_{V4}^G = \dot{n}_{V^{4+}}^P \tag{2.7}$$

$$\dot{n}_{V^{5+}}^G = -\dot{n}_{V^{5+}}^C \tag{2.8}$$

If an ideal mixing is assumed for the reactor (R) and for the positive tank (+T), the following substitution can be done:

$$\dot{n}_i^{in} = \dot{n}_i^{+T} \tag{2.9}$$

$$\dot{n}_i^{out} = \dot{n}_i^R \ . \tag{2.10}$$

Moreover, since the stoichiometric ratio between V^{5+} and V^{4+} is 1 (for each mole consumed of V^{5+}, one mole of V^{4+} is produced) the generation terms are the same:

$$\dot{n}_{V^{5+}}^C = -\dot{n}_{V^{4+}}^P \ . \tag{2.11}$$

The generation term can also be expressed as function of the current that is provided in the regeneration reactor. In fact, by applying the Faraday's law, it is possible to obtain the following equation:

$$\dot{n}_i^G = \frac{i_R}{F} \tag{2.12}$$

Where i_R is the current provided by the battery test system in the regeneration reactor and F is the faraday constant. Therefore, equation (2.6) and (2.7) become:

$$\frac{dN_{V^{5+}}^{R}}{dt} = \dot{n}_{V^{5+}}^{+T} - \dot{n}_{V^{5+}}^{R} - \frac{i_R}{F} \tag{2.13}$$

$$\frac{dN_{V^{4+}}^{R}}{dt} = \dot{n}_{V^{4+}}^{+T} - \dot{n}_{V^{4+}}^{R} + \frac{i_R}{F} \tag{2.14}$$

2.5.2.2 Positive Tank

The mass balance of V^{5+} and V^{4+} in the positive tank can be represented by the following equation:

$$\frac{dN_i^{+T}}{dt} = \dot{n}_i^{in,1} + \dot{n}_i^{in,2} - \dot{n}_i^{out,1} - \dot{n}_i^{out,2} \tag{2.15}$$

Where,

- $\frac{dN_i^{+T}}{dt}$ = accumulation term for the generic ion *i* in the positive tank ;
- $\dot{n}_i^{in,1}$ = inlet molar flow rate for the generic ion *i* from line 1;
- $\dot{n}_i^{in,2}$ = inlet molar flow rate for the generic ion *i* from line 2;
- $\dot{n}_i^{out,1}$ = outlet molar flow rate for the generic ion *i* from line 1;
- $\dot{n}_i^{out,2}$ = outlet molar flow rate for the generic ion *i* from line 2;

Line 1 is the line which comes from the regeneration reactor, line 2 is the line which comes from the VRFB cell. By assuming an ideal mixing for both the regeneration reactor, the VRFB cell and the positive tank, the following equation is obtained:

$$\frac{dN_i^{+T}}{dt} = \dot{n}_i^{R} + \dot{n}_i^{VRFB} - \dot{n}_i^{+T} - \dot{n}_i^{+T} \tag{2.16}$$

Rearranging the equation (2.16), the result for both the V^{5+} and V^{4+} ions is:

$$\frac{dN_{V^{5+}}^{+T}}{dt} = \dot{n}_{V^{5+}}^{R} + \dot{n}_{V^{5+}}^{VRFB} - 2\dot{n}_{V^{5+}}^{+T} \tag{2.17}$$

$$\frac{dN_{V^{4+}}^{+T}}{dt} = \dot{n}_{V^{4+}}^{R} + \dot{n}_{V^{4+}}^{VRFB} - 2\dot{n}_{V^{4+}}^{+T} \tag{2.18}$$

2.5.2.3 VRFB cell

The VRFB cell is divided in two half-cell: in one side only V^{5+} and V^{4+} ions are present, in the other one, V^{3+} and V^{2+}. Therefore, 4 different mass balances can be written with the following equation:

$$\frac{dN_i^{VRFB}}{dt} = \dot{n}_i^{in} - \dot{n}_i^{out} + \dot{n}_i^{G} \tag{2.19}$$

Where $\frac{dN_i^{VRFB}}{dt}$ is the accumulation term for the generic ion *i* in the VRFB cell. Also for these mass balances, since the stoichiometric ratio for each ion in the electrochemical reactions is one, is it possible to write the following equation:

$$\dot{n}_i^{G} = \dot{n}_{V^{5+}}^{P} = -\dot{n}_{V^{4+}}^{C} = -\dot{n}_{V3}^{C} = \dot{n}_{V2}^{P} \tag{2.20}$$

As it has been done for the regeneration reactor, by applying the Faraday's law, it is possible to rewrite the generation term in the following way:

$$\dot{n}_i^{G} = \frac{i_{VRFB}}{F}, \qquad i_{VRFB} = i_+ = i_- \tag{2.21}$$

Where i_{VRFB} is the current which circulates inside of positive electrode (i_+) and inside of the negative eletcrode (i_-). The positive current depends on the concentration of the ions in the catholyte, according to the Butler-Volmer equation:

$$i_+ = Ai_{0,+}\left\{\exp\left(\frac{(1-\alpha_+)zF\eta_+}{RT}\right) - \exp\left(-\frac{\alpha_+ zF\eta_+}{RT}\right)\right\} \tag{2.22}$$

$$i_{0,+} = zFk_+(c_{V^{4+}})^{1-\alpha_+}(c_{V^{5+}})^{\alpha_+} \tag{2.23}$$

Where A is the specific surface area (SI unit: m^3/m^2) of the porous electrode, α_+ is the transfer coefficient (dimensionless) and k_+ is the rate constant (SI unit: m/s). The overpotential, η_+ (SI unit: V), is defined as:

$$\eta_+ = \varphi_s - \varphi_e - E_{eq} \tag{2.24}$$

Where φ_s is the electric potential of the solid phase of the electrode (SI unit: V), φ_e is the electrolyte potential (SI unit: V) and E_{eq} is the equilibrium potential calculated trough the Nernst's equation. The same equations can be written also for the negative electrode reaction, where the same form of Butler-Volmer equation is used.

$$i_- = Ai_{0,-}\left\{\exp\left(\frac{(1-\alpha_-)zF\eta_-}{RT}\right) - \exp\left(-\frac{\alpha_- zF\eta_-}{RT}\right)\right\} \tag{2.25}$$

$$i_{0,-} = zFk_-(c_{V^{2+}})^{1-\alpha_-}(c_{V^{3+}})^{\alpha_-} \tag{2.26}$$

The previous form of Butler-Volmer equation is valid when the electrode reaction is controlled by electrical charge transfer at the electrode and not by the mass transfer to or from the electrode surface from or to the bulk electrolyte.

In Tab. 2.1 are reported all the numerical values of the parameters used in the previous formulas. The only exception is related to the positive and negative overpotentials, which depends on the SoC of the catholyte and of the anolyte respectively. Therefore, an empirical model is needed.

Table 2.4: *Values of the constants used in the Butler-Volmer equation [17].*

Parameters	Values
α_+ [-]	0,55
α_- [-]	0,45
k_+ [m/s]	$3{,}5e^{-8}$
k- [m/s]	$7{,}2e^{-8}$
A [$cm^{2]}$	40
F [C/mol]	96485
R [J/(mol*K)]	8,31
T [K]	293,15

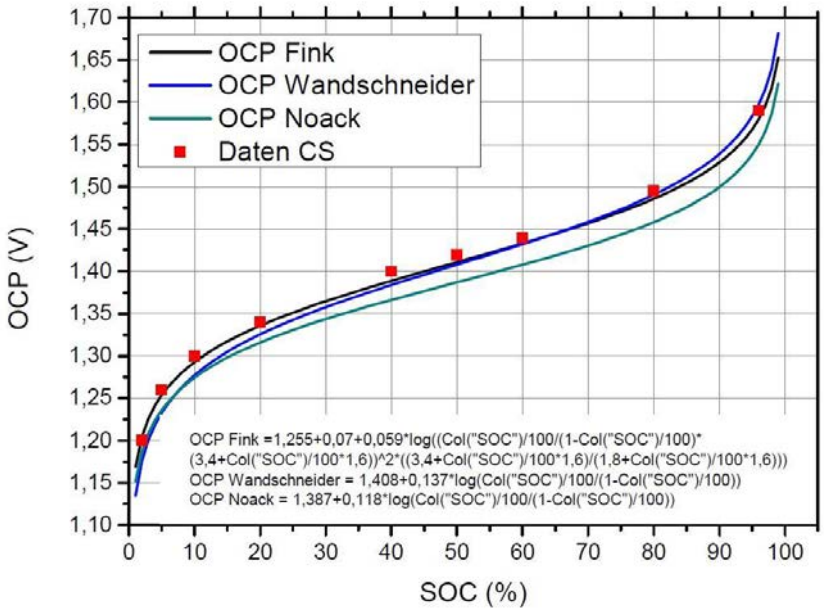

Figure 2.12: *Empirical functions for open circuit potential depending of the state of charge [19].*

The overpotential can be also expressed in the following way:

$$\eta = E_{exp} - E_{eq} \tag{2.27}$$

Where E_{exp} is the cell voltage which is measured by instruments, in this case, the battery test system. The equilibrium potential E_{eq}, also called OCV (open circuit voltage), can be expressed by a function which depends only on the SoC of the electrolyte, as it is shown in Fig. 2.12. In this study, the OCP Fink function was used to calculate the overpotential of the anolyte and of the catholyte by using the corresponding SoC. This means that, since the cell voltage is constant during the charging, because at the point in which the regeneration process is turned on, the VRFB cell is charged potentiostatically, the overpotential for the anolyte and the catholyte can be express with the following equations:

$$\eta_+ = 1.65 - OCP_{Fink}\, f(SoC_+) \tag{2.28}$$

$$\eta_- = 1.65 - OCP_{Fink}\, f(SoC_-) \tag{2.29}$$

Where the SoC of the anolyte and of the catholyte are defined in this way:

$$SoC_+ = \frac{C_{V^{5+}}^{VRFB}}{C_{V^{5+}}^{VRFB} + C_{V^{4+}}^{VRFB}} \tag{2.30}$$

$$SoC_- = \frac{C_{V^{2+}}^{VRFB}}{C_{V^{2+}}^{VRFB} + C_{V^{3+}}^{VRFB}} \tag{2.31}$$

Finally, the four mass balances for the VRFB cell are described by the following equations:

$$\frac{dN_{V^{5+}}^{VRFB}}{dt} = \dot{n}_{V^{5+}}^{+T} - \dot{n}_{V^{5+}}^{VRFB} + \frac{i_+}{F} \tag{2.32}$$

$$\frac{dN_{V^{4+}}^{VRFB}}{dt} = \dot{n}_{V^{4+}}^{+T} - \dot{n}_{V^{4+}}^{VRFB} + \frac{i_+}{F} \tag{2.33}$$

$$\frac{dN_{V^{3+}}^{VRFB}}{dt} = \dot{n}_{V^{3+}}^{-T} - \dot{n}_{V^{3+}}^{VRFB} - \frac{i_-}{F} \tag{2.34}$$

$$\frac{dN_{V^{2+}}^{VRFB}}{dt} = \dot{n}_{V^{2+}}^{-T} - \dot{n}_{V^{2+}}^{VRFB} + \frac{i_-}{F} \tag{2.35}$$

2.5.2.4 Negative Tank

The rationale to obtain the mass balance equations for the negative tank is very similar to the one presented in paragraph §2.5.1.2, where the mass balance equations for the positive tank were described. The only difference is that for the negative tank there is only one outlet and one inlet as it is shown in Fig. 2.10 and the ions are the one of the anolyte. Therefore, the mass balances for the negative tank becomes:

$$\frac{dN_{V^{3+}}^{-T}}{dt} = \dot{n}_{V^{3+}}^{VRFB} - \dot{n}_{V^{3+}}^{-T} \tag{2.36}$$

$$\frac{dN_{V^{2+}}^{-T}}{dt} = \dot{n}_{V^{2+}}^{VRFB} - \dot{n}_{V^{2+}}^{-T} \tag{2.37}$$

On the next page a list of all the described equations is presented, where the number of moles is substituted with the concentration, assuming that the volume and the density are constant along the time and the letter doesn't change between the anolyte and the catholyte. The result of the last assumption allows to consider the volumetric flowrate of the positive and negative tank equal.

Regeneration reactor

$$\tau \frac{dc_{V^{5+}}^{R}}{dt} = c_{V^{5+}}^{+T} - c_{V^{5+}}^{R} - \frac{i_R}{\dot{V}F} \tag{2.38}$$

$$\tau \frac{dc_{V^{4+}}^{R}}{dt} = c_{V^{4+}}^{+T} - c_{V^{4+}}^{R} + \frac{i_R}{\dot{V}F} \quad , \tag{2.39}$$

Positive tank

$$\tau \frac{dc_{V^{5+}}^{+T}}{dt} = c_{V^{5+}}^{VRFB} + c_{V^{5+}}^{R} - 2c_{V^{5+}}^{+T} \tag{2.40}$$

$$\tau \frac{dc_{V^{4+}}^{+T}}{dt} = c_{V^{4+}}^{VRFB} + c_{V^{4+}}^{R} - 2c_{V^{4+}}^{+T} \quad , \tag{2.41}$$

VRFB cell

$$\tau \frac{dc_{V^{5+}}^{VRFB}}{dt} = c_{V^{5+}}^{+T} - c_{V^{5+}}^{VRFB} + \frac{i_+}{\dot{V}F} \tag{2.42}$$

$$\tau \frac{dc_{V^{4+}}^{VRFB}}{dt} = c_{V^{4+}}^{+T} - c_{V^{4+}}^{VRFB} + \frac{i_+}{\dot{V}F} \tag{2.43}$$

$$\tau \frac{dc_{V^{3+}}^{VRFB}}{dt} = c_{V^{3+}}^{-T} - c_{V^{3+}}^{VRFB} - \frac{i_-}{\dot{V}F} \tag{2.44}$$

$$\tau \frac{dc_{V^{2+}}^{VRFB}}{dt} = c_{V^{2+}}^{-T} - c_{V^{2+}}^{VRFB} + \frac{i_-}{\dot{V}F} \quad , \tag{2.45}$$

Negative tank

$$\tau \frac{dc_{V^{3+}}^{-T}}{dt} = c_{V^{3+}}^{VRFB} - c_{V^{3+}}^{-T} \tag{2.46}$$

$$\tau \frac{dc_{V^{2+}}^{-T}}{dt} = c_{V^{2+}}^{VRFB} - c_{V^{2+}}^{-T} \quad . \tag{2.47}$$

Where τ (SI unit: min) is the ratio between the volume (80 mL) and the volumetric flowrate (165 mL/min). In Tab. 2.5 the ten initial conditions necessary to solve all these ordinary differential equations are stated. The solution has been calculated by using Matlab® (See App. A for the scripts)

Table 2.5: *Initial conditions to solve the ordinary differential equations.*

Variable	$c_{V^{5+}}^{R}$	$c_{V^{4+}}^{R}$	$c_{V^{5+}}^{+T}$	$c_{V^{4+}}^{+T}$	$c_{V^{5+}}^{VRFB}$	$c_{V^{4+}}^{VRFB}$	$c_{V^{3+}}^{VRFB}$	$c_{V^{2+}}^{VRFB}$	$c_{V^{3+}}^{-T}$	$c_{V^{2+}}^{-T}$
Value at t = 0s [kmol/m^3]	1,624	0	1,624	0	1,624	0	0,182	1,442	0,182	1.442

2.5.2.5 Results

Fig. 2.13 shows three result plots, as function of time: in the left one the concentration of V^{5+} and V^{4+} in the catholyte, in the right one the concentration of V^{3+} and V^{2+} in the anolyte and, finally, in the middle one the current in the positive electrode of VRFB (i_+), the current in the negative electrode of VRFB (i_-) and the current that circulates in the regeneration reactor (here indicated with i_{DSA}). The latter is constant because in the regeneration reactor a constant current equal to 1 A is provided. As it can be seen in the catholyte, the concentration of V^{5+} decreases along the time just like the concentration of V^{2+} in the anolyte. This happens because V^{4+} ions, which are produced in the regeneration reactor, are pumped in the VRFB cell to be oxidized: this leads to reduction of the V^{3+} ions in the negative tank in order to rebalance the electrolyte. Indeed, the concentration of V^{3+} goes to zero after around three hours. To further understand the current behaviour, Fig. 2.14 also depicts V3+ and V4+ concentrations: here the same data are plotted. in the upper plot, only the concentration of V^{4+} in the catholyte and the concentration of V^{3+} in the anolyte are reported in order to underline their intersect point. Before this point the concentration of V^{4+} is lower than the concentration of V^{3+}, therefore, the ions in the catholyte conduct a current which is lower than the anolyte one. Therefore, since the current in the VRFB cell has to be always the same between the two half-cell, the behaviour that characterizes the real current, before the intersect point, is the one shown by the positive one, i_+.

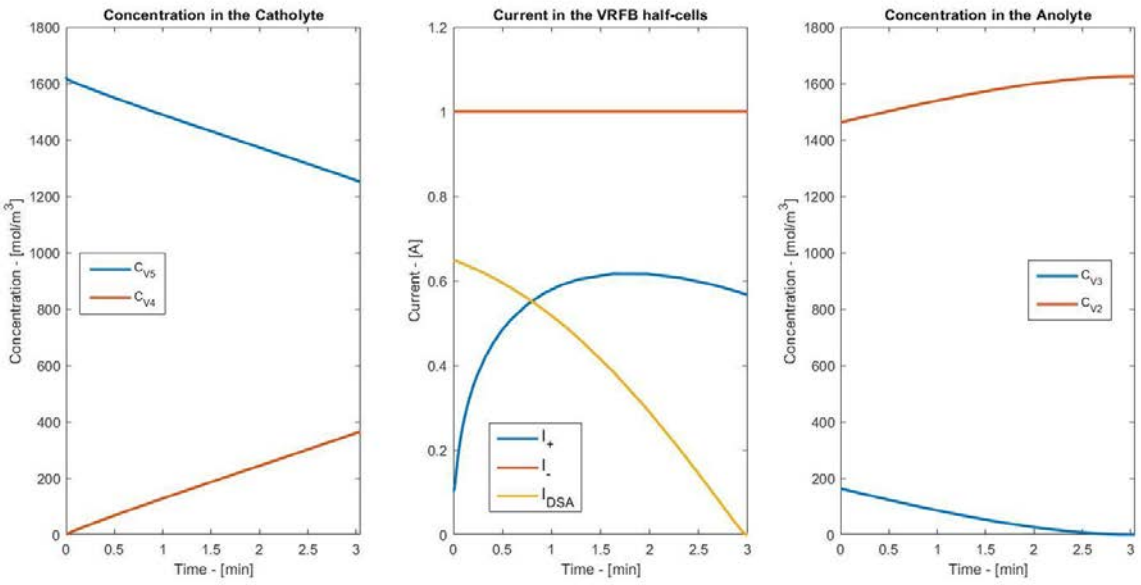

Figure 2.13: *(Left) Concentrations in the Catholyte; (Middle) Currents in the positive and negative electrode of the VRFB cell and in the regeneration reactor (i_{DSA}); (Right) Concentration in the Anolyte.*

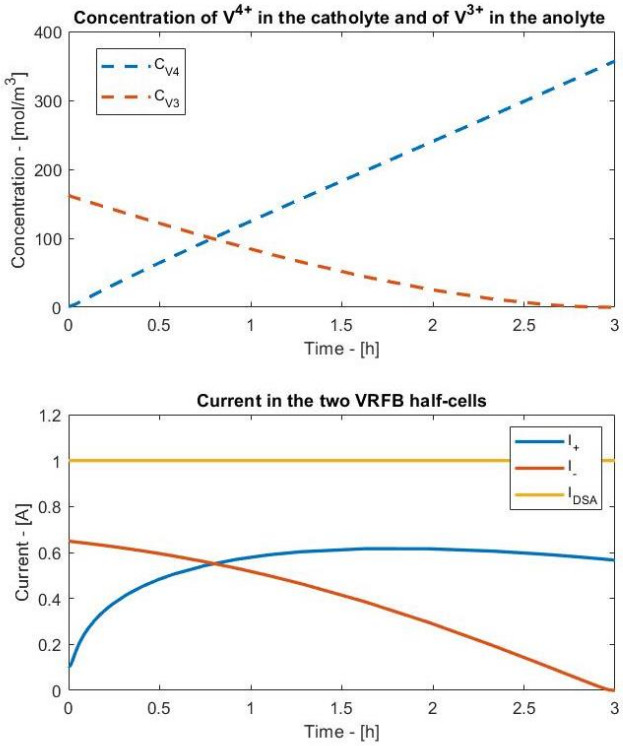

Figure 2.14: *(Top) Concentration of V^{3+} and V^{4+} in the anolyte and catholyte respectively as function of time. (Bottom) behaviour of the positive and negative current in both half-cells of the VRFB and of the current in the regeneration reactor (i_{DSA}) as function of time.*

But, as soon as the V^{3+} ions start to conduct a current lower than the catholyte one, the behaviour of the current inside of the cell is well described by the negative one, i.. Therefore, the current of the cell shows a peak exactly when there is a changing in the mass limitation between the catholyte and the anolyte, namely when the concentration of V^{4+} becomes lower than the concentration of V^{3+}. This model can justify the real behaviour of the current shown in Fig. 2.15: here, the model is compared with the current measured by the battery test system. The plot shows that at first, the current measured during the experiment follows the one in the positive electrode, because it is the side where the mass limitation comes from, namely the catholyte. But then, as soon as the concentration of V^{3+} doesn't allow the anolyte to sustain the same current of the catholyte in its half-cell, the current in the cell starts decreasing by following the negative one. Therefore, the result obtained by the mathematical model can be used to find a suitable end point of the regeneration process. Indeed, as discussed in the previous paragraph, if the regeneration process doesn't stop in the right moment, an overshoot takes place and the rebalance is not reached. If the regeneration process is turned off when the concentration of V^{4+} in the catholyte is equal to the concentration of V^{3+} in the anolyte, the overshoot should be avoided. In other words, the exact moment to stop the production of V^{4+} is when the current in the cell reaches its maximum value.

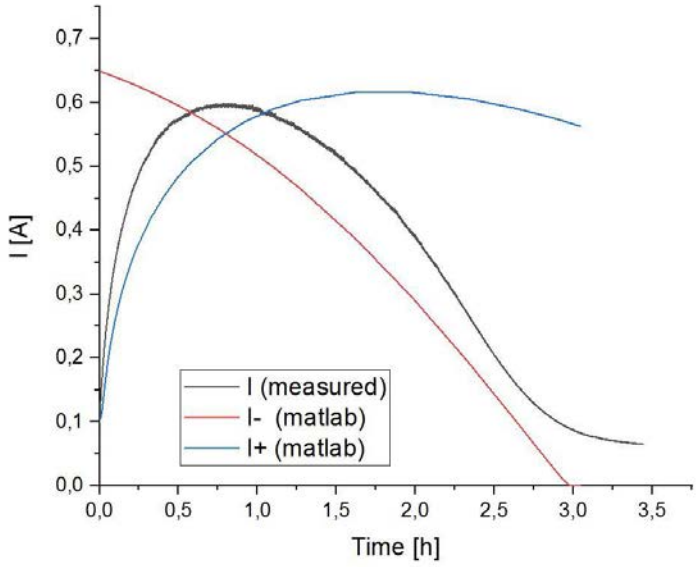

Figure 2.15: *Comparison between the real current measured by the battery test system and the current calculated by the mathematical model solved with Matlab with an initial shift of 20%*

The same experiment, then, has been repeated by using a different initial shift: 10% and 30%. In the left plot of Fig. 2.16 one can observe that, both with an initial shift of 10% (left) and 30% (right), the mathematical model can justify the dynamics behaviour of the current in the VRFB cell. What it has changed respect to Fig. 2.15 is the interval time in which the current reaches a steady-state condition and the value of the maximum point: for the lower initial shift the maximum current measured by the battery test

system is 0,482 A and the transient dies out after 1.8 hours, for the higher initial shift, instead, the maximum current is 0,629A and the transient dies out after at least 5 hours.

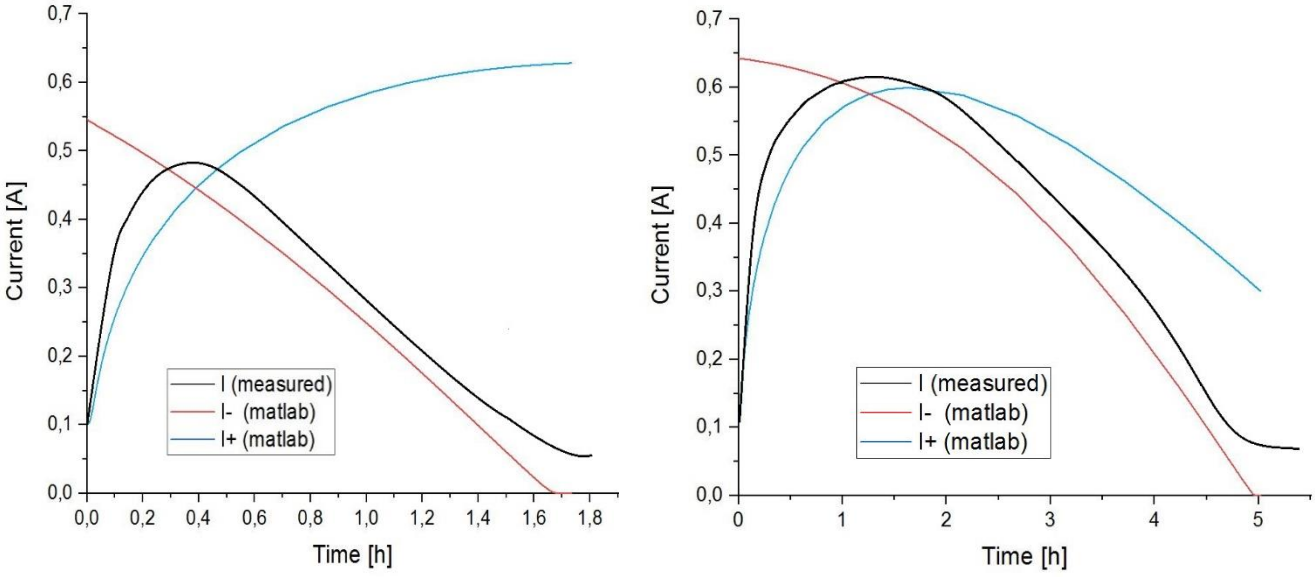

Figure 2.16: *comparison between the real current measured by the battery test system and the current calculated by the mathematical model solved with Matlab, with an initial shift of 10% (left) and 30% (right).*

In the next paragraph the same experiment described in §2.5.1 has been performed (with an initial shift of 20%), with the difference that the regeneration process has been stopped as soon as the current in the VRFB cell reached a maximum point.

2.5.3 A suitable end-point criterion

As introduced in the previous paragraph, the mathematical model developed before, suggests a suitable end-point criterion for stopping the regeneration process avoiding the overshoot. For this reason, the same experiments discussed in §2.5.1 has been realized, with the difference that the regeneration process has been stopped as soon as the current reached the maximum point, as shown in Fig. 2.17. By measuring the composition of the electrolyte at the end of the process, it is possible observing that the composition of V^{+3} is still higher than the composition of V^{4+} and therefore, an overshoot of 3,2% is still present, as reported in Tab. 2.6. The reason of this lower overshoot is related to a delate of the concentration of V^{4+} that appears in the cell in respect to the concentration in the regeneration reactor. Indeed, as it is shown in Fig. 2.18, when the current is at the maximum point, the concentration in the cell is 101,5 mol/m^3, while the concentration in the reactor is around 109 mol/m^3. Therefore, even though the regeneration reactor has been stopped after 0,8 h, due to the time delay of the cell in respect to the reactor, the concentration of V^{4+} in the catholyte will reach the value of 109 mol/m^3, and an overshoot will take place. In order to avoid the overshoot, this delayed time has to be considered. For this reason, the regeneration process should be stopped 0,06 h (~ 4 min) before the maximum point appears.

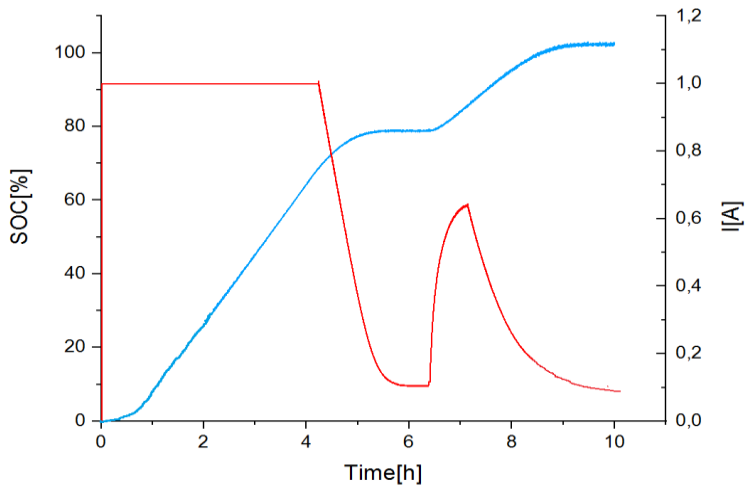

Figure 2.17: *Behaviour of the current in the VRFB cell (red line) and behaviour of the negative SoC (blue line) as function of time.*

Table 2.6: *Comparison between the two experiments performed: the first without an end-point criterion, the second with an end-point criterion suggested by the mathematical model.*

	V^{3+} [%]	V^{4+} [%]
Before the regeneration	40	60
After the regeneration (without an end-point criterion)	76,35	23,65
After the regeneration (with an end-point criterion)	53,2	46,8

But this can be done only if the initial shift is known, otherwise it is not possible knowing when the maximum point appears. Even though an overshoot still took place, this is very small (3.2%) respect to the one obtained before (20%), Having an overshoot as small as the one obtained causes an imbalance between the anolyte and the catholyte at the beginning, but since the V^{+3} may be oxidized during long-term performance, the electrolyte can be rebalanced back without any additional process. Therefore, the maximum value of the current can be a suitable end-point for the regeneration process.

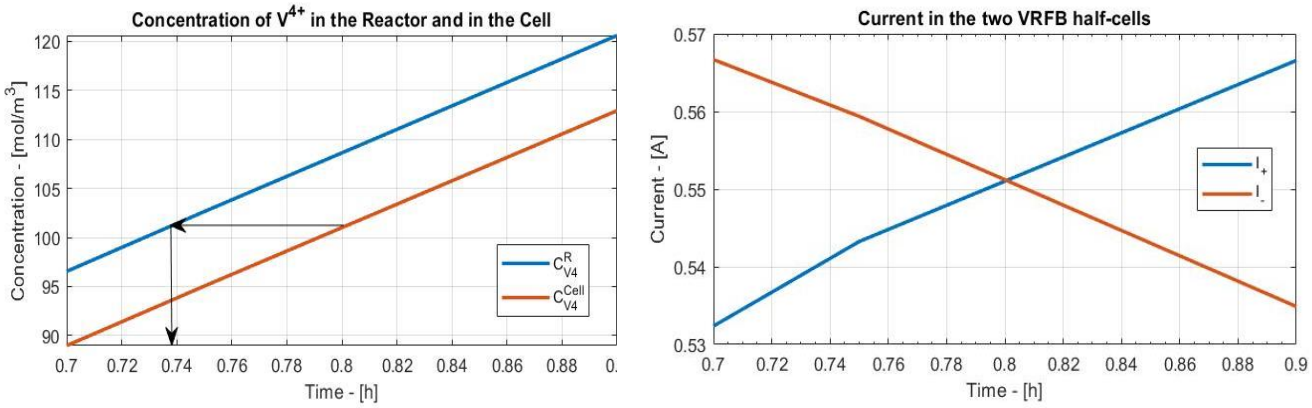

Figure 2.18: *Concentration of V^{4+} in the regeneration reactor and in the cell (left); behaviour of the positive and negative current in both half-cells of the VRFB (right).*

Chapter 3

Economic Analysis

An economic analysis is necessary in order to estimate the cost of the regeneration process. In this chapter different costs will be described: the cost for a generic plant of vanadium redox flow batteries, divided in power cost, energy cost and pumping cost and the cost for a suitable regeneration process. Finally, a numerical example will be discussed.

3.1 VRFB system cost

Since the power and the energy can be scaled independently, the overall cost of a VRFB can be described by the following equation [20]:

$$C_{VRFB} = C_{Power} + C_{Energy} + C_{pumping} \tag{3.1}$$

The cost for the power is related to the number of the stacks and therefore to their single components, which are shown in Fig. 3.1. The cost of the energy is related to the electrolyte volume (the storage media) and the concentration of the active species. Finally, the cost for the pumping depends on the volumetric flowrate and on the efficiency of the pump.

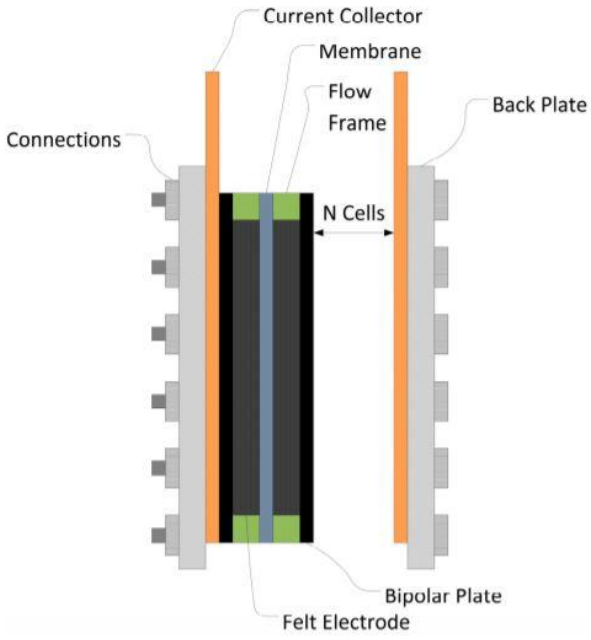

Figure 3.1: *Components and layout of a redox flow battery stack [20].*

3.1.1 Power cost

All components except the electrolyte solution and the tank are power components. The overall costs of the power components can be summarized by the following formula:

$$C_{Power} = C_{Stack} + C_{Control\ engineering} + C_{Fluid\ regulation} + C_{Power\ Assembling} \tag{3.2}$$

All the components are needed for the operation of the battery, but only the stack is directly involved in the energy conversion. The previous parts can be broken down into further components:

$$\begin{gathered} C_{Fluid\ regulation} = C_{Pumps} + C_{Piping} + C_{Valves} \\ C_{Control\ engineering} = C_{Sensor} + C_{Actuator} + C_{Thermal\ regulation} \\ C_{Stack} = C_{BPP} + C_{Felt} + C_{Gasket} + C_{Membrane} + C_{Frame} + C_{End\ plate} + C_{Isolation\ plate} \\ + C_{Current\ cullector} + C_{Connections} + C_{Stack,Assembling} \end{gathered} \tag{3.3}$$

The stack components are of great interest as they directly influence the performance of the battery. In simplified terms the cost of one stack is a function of cell number (N) and cell size (A_{Active}):

$$\begin{gathered} C_{Stack}(N, A_{Active}) = (N+1) * A_{Active} * c_{BPP} + 2N * A_{Active} * (c_{Felt} + c_{Gasket} + c_{Frame}) \\ + A_{Active} * (c_{End\ plate} + c_{Current\ cullector} + c_{Isolation\ plate}) \\ + C_{Connections} + C_{Stack,Assembling} + N * A_{Active} * c_{Membrane} \end{gathered} \tag{3.4}$$

Where c_i is the specific cost per unit of area [€/m^2]. The production costs of the system $C_{Power\ Assembling}$ or of the stack $C_{Stack,Assembling}$ could be calculated using the necessary man-hours, specific man-hours costs and the specific energy cost:

$$C_{Assembling} = t_{manhours} * (C_{manhour} + c_{Energy}) \tag{3.5}$$

For the configuration of a battery system, the output power of the battery is the first variable that has to be specified. The next step is to determine either the cell size (A_{active}) or the number of the cells. The output mean power $\bar{P}$ and a design current i are determined first, then, if the cell area (A_{active}) is specified, the number of the cell can be obtained in the following way:

$$N = \frac{\bar{P}}{i * \overline{U_{cell}}} \tag{3.6}$$

Where $\overline{U_{cell}}$ is the average cell voltage, which depends on the effective cell voltage and on the used SoC range according the following equation:

$$\overline{U_{cell}} = \frac{1}{SoC_{max} - SoC_{min}} \int_{SoC_{min}}^{SoC_{max}} U_{cell} dSoC \tag{3.7}$$

The effective cell voltage U_{cell} is calculated as the reversible cell voltage (U_{rev}) subtracted by all losses inside the cell:

$$U_{cell} = U_{rev} - U_{act} - U_{con} - U_{ohm} \tag{3.8}$$

Where U_{act} is the activation overpotential, U_{conc} is the concentration overpotential and U_{ohm} is the ohmic overpotential (See App. C for further explanation).
Therefore, the stack cost becomes:

$$\begin{aligned} C_{Stack}(\overline{P}) = & \left(\frac{\overline{P}}{i * \overline{U_{cell}}} * A_{Active} + A_{Active}\right) * c_{BPP} \\ & + 2\frac{\overline{P}}{i * \overline{U_{cell}}} * A_{Active} * A_{Active} * (c_{Felt} + c_{Gasket} + c_{Frame}) \\ & + A_{Active} * \left(c_{End\ plate} + c_{Current\ cullector} + c_{Isolation\ plate}\right) \\ & + C_{Connections} + C_{Stack,Assembling} + \frac{\overline{P}}{i * \overline{U_{cell}}} * A_{Active} * c_{Membrane} \end{aligned} \tag{3.9}$$

The costs of the single components have to be defined in detail. As many parts of RFBs cannot bought from the market, costs were composed of material costs (MC), either specific as costs per m^2 or kg,

$$\begin{aligned} C_{End\ plate} &= X_{End\ plate} * \frac{MC_{End\ plate}}{m^2} + n_{End\ plate} * C_{Fabr.\ End\ plate} \\ C_{Isolation\ plate} &= X_{Isolation\ plate} * \frac{MC_{Isolation\ plate}}{m^2} + n_{Isolation\ plate} * C_{Fabr.\ Isolation\ plate} \\ C_{Current\ collector} &= X_{Current\ collector} * \frac{MC_{Current\ collector}}{m^2} + n_{Current\ collector} * C_{Fabr.\ Current\ collector} \\ C_{Bipolar\ plate} &= X_{Bipolar\ plate} * \frac{MC_{Bipolar\ plate}}{m^2} + n_{Bipolar\ plate} * C_{Fabr.\ Bipolar\ plate} \\ C_{Felt} &= X_{Felt} * \frac{MC_{Felt}}{m^2} + n_{Felt} * C_{Fabr.\ Felt} \\ C_{Frame} &= X_{Frame} * \frac{MC_{Frame}}{m^2} + n_{Frame} * C_{Fabr.\ Frame} \end{aligned} \tag{3.10}$$

$$C_{Gasket} = X_{Gasket} * \frac{MC_{Gasket}}{m^2} + n_{Gasket} * C_{Fabr.\ Gasket}$$

$$C_{Membrane} = X_{Membrane} * \frac{MC_{Membrane}}{m^2} + n_{Membrane} * C_{Fabr.\ Membrane}$$

or as costs per unit, and fabrication costs (FC). Most components do not have the same size as the active cell area. One also has to take into account that parts of the material are wasted during fabrication, so a factor for the real material demand per active cell area was needed for that reason. This factor can either be proportional or fixed. In this case, the factor ($X_{component}$) was supposed to be fixed to the active cell area. The following equation are therefore obtained:

3.1.2 Energy cost

The costs of energy consist of electrolyte and tanks costs:

$$C_{Energy} = C_{Electrolyte} + C_{Tank} \tag{3.11}$$

The electrolyte costs regard the costs of the active species, the costs of the solvent, the costs of additives and the costs of fabrication:

$$C_{Electrolyte} = C_{Active\ Material} + C_{Solvent} + C_{Additive} + C_{Electrolyte\ Fabrication} \tag{3.12}$$

The costs of the electrolyte scale with the volume. The required volume is directly dependent on the energy that has to be stored. The volume of the electrolyte for the required energy capacity for one tank is calculated as follows:

$$V = \frac{Energy}{\overline{U_{cell}} * SoC\ range * \frac{F * z * c}{3600}} \tag{3.13}$$

Where $SoC\ range$ is the usable state of charge, F is the Faraday's constant, z is the number of electron equivalents per mol and c is the molar concentration of vanadium species [mol/L].

The useable state of charge range is a factor that takes into account the fact that the battery is never fully charged or discharged, so not all potentially available capacity can be utilized. This means that a substantial amount of the active species cannot be used for storing energy. As the calculated volume is needed for either the cathode or anode, this volume has to be multiplied by two for the calculation of the total electrolyte amount. The total electrolyte costs could be calculated by the following equation:

$$C_{Electrolyte} = 2 * V * [(c * C)_{Active\ Material} + (c * C)_{Solvent} + (c * C)_{Additive}] + C_{Electrolyte\ Fabrication} \tag{3.14}$$

Where c is the vanadium concentration [mol/l] and C is the specific cost [€/mol].

3.1.3 Pumping cost

The energy demand required for transporting the electrolyte in and out of the stacks, is a significant source of power loss in a flow battery. Furthermore, hydraulic, electric and electrochemical subsystems are closely interrelated. A higher flow rate decreases the concentration overpotential but increases the pump power demand. Long and narrow inlet and outlet channels of the cells reduce shunt currents, but increase the hydraulic resistance and thus again the pump power demand.

In this analysis, two pumps have been considered to apply the desired volumetric flow rate to the two electrolyte circuits. The required electric pump power is calculated with equation (3.15) considering the flow rate dependent pump efficiency as variable.

$$P_{Pumps}[W] = 2\,\frac{\Delta p_{Total} Q_{Pump}}{\eta_{Pump}} \tag{3.15}$$

Where Δp_{Total} is the total pressure drop due to the hydraulic circuit of the battery, Q_{Pump} is the pump volumetric flow rate, η_{Pump} is the pump efficiency and P_{Pumps} is the electric pump power of both the pumps.

The efficiency of the pump strongly depends on the flow rate, as shown in Fig. 3.2. The presented curves are derived from datasheets of seven different pumps from three different manufacturers [21]. All efficiencies are derived while pumping water, not VRFB electrolyte. The pump efficiency for pumping electrolyte has not been published yet. The efficiencies of pumps from different manufacturers show a similar trend with a peak efficiency at approximately 60 % of the maximum flow rate. This point is called best efficiency-point (BEP). However, the efficiencies of different pumps in their BEPs vary strongly. Therefore, it is necessary calculating an average efficiency value [21].

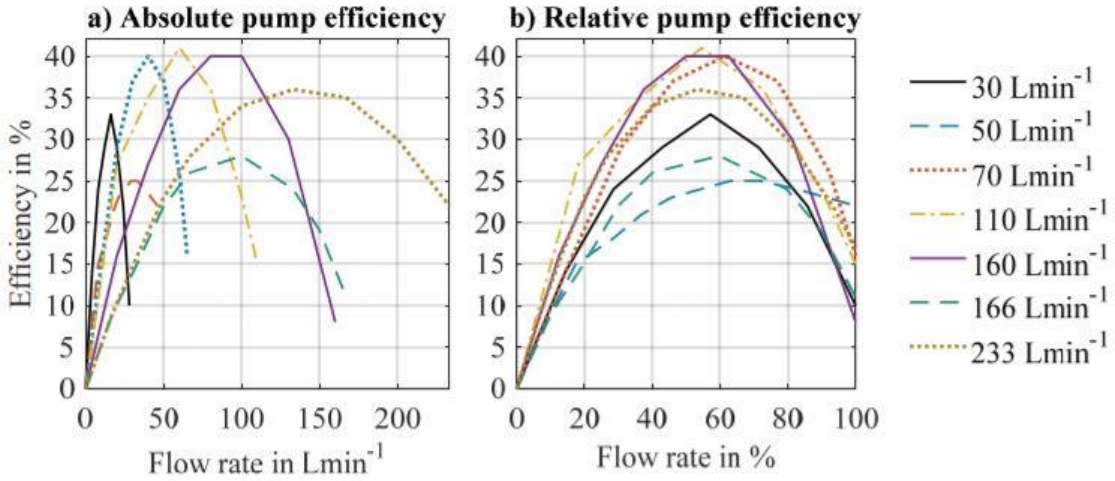

Figure 3.2: *Pump efficiency over rated flow rate [21].*

3.1.3.1 Pressure drops

The pressure drops in the cell are due to the resistance in the input channel, distribution funnel, porous flow-through electrode, collection funnel and output channel, as showed in the following equation [21]:

$$\Delta p_{Total} = \Delta p_{Orifices} + \Delta p_{Pipes} + \Delta p_{Channels} + \Delta p_{Electrode} \quad (3.16)$$

For each of these pressure drops, semi-empirical equations exist:

- Pressure drop in the orifices

  The orifices such as bends, T-junctions, tank inlet and outlet, valves, and sensors cause a pressure drop which can be calculated with the following equation [21]:

$$\Delta p_{Orifice} = 8k_L \frac{\rho_{El}}{{d_{orif}}^4 \pi^2} {Q_{Orif}}^2 \quad (3.17)$$

  Where k_L is the loss coefficient, ρ_{El} is the electrolyte density, d_{orif} is the diameter of the orifice and Q_{Orif} is the flowrate through the orifice. There are different values of k_L depending on the hydraulic elements as presented in Tab. 3.1.

Table 3.1: *Loss coefficients for various hydraulic elements [21].*

Component	k_L
90° bend	0,30
T-junction, direct flow	0,20
T-junction, branch flow	1
Tank, inlet	1
Tank, outlet	0,42

- Pressure drop in pipes

  The pressure drops in pipes can be obtained by using the following equation [21]:

$$\Delta p_{Pipe} = 8f \frac{l_p \rho_{El}}{{d_P}^5 \pi^2} {Q_P}^2 \quad (3.18)$$

  Where f is the friction factor, l_p is the pipe length, d_P is the pipe diameter and Q_P is the volumetric flowrate through the pipe. The definition of the friction factor depends on the flow regime. If the Reynolds number is below 2,300, the flow is supposed to be laminar. Thus, the

friction factor only depends on a shape factor and the Reynolds number, as shown in Eq. (3.19). For a circular cross-section, the shape factor is 64. For a Reynolds number beyond 4,000, we assume the flow to be fully turbulent. The friction factor now depends on the Reynolds number and the internal roughness height. Between a Reynolds number of 2,300 and 4,000, a linear transition region between the laminar and the turbulent behaviour is assumed. The Reynolds number is computed as shown in Eq. (3.20).

$$f = \begin{cases} {}^{64}/_{Re_P}, & \text{for } Re_P \leq 2{,}300 \\ f_{La} + \frac{f_{Tu} - f_{La}}{2{,}300}(Re_P - 2{,}300), & \text{for } 2{,}300 < Re_P \leq 4{,}000 \\ \left(1.8 \log_{10}\left({}^{6.9}/_{Re_P} + \left(\frac{{}^{\epsilon}/_{d_P}}{3.7}\right)^{1.11}\right)\right)^{-2}, & \text{for } 4{,}000 \leq Re_P \end{cases} \tag{3.19}$$

$$Re_P = 4\,\frac{\rho_{EI} Q_P}{\mu_{EI} \pi d_P} \tag{3.20}$$

Where Re_P is th Reynolds number in the pipe, f_{La} is the friction factor at Re_P = 2300 and f_{Tu} is the friction factor at Re_P = 4000 [21].

- Pressure drop in the channels

The straight channel parts are a linear hydraulic resistance if they carry a laminar flow, which is desired to keep the pressure drops low. The orifices in the channel, such as 90° and 180° bends show a quadratic dependence on the flow rate, as shown in Eq. (3.21). Hence, the function shown in Eq. (3.21) is proposed to model the non-linear hydraulic resistance of the channels in the cell [21].

$$\Delta p_{Channel} = \beta Q_C + \gamma Q_C^2 \tag{3.21}$$

The values of β and γ depend on several factors as shown in Tab. 3.2.

Table 3.2: *Coefficients β and γ for calculation the non-linear hydraulic resistance of the channels according to equation (3.21). [21].*

Design	Electrode area	Meander count	Channel width	β in 10^7 Pa·s·m^{-3}	γ in 10^9 Pa·(s·m^3)^2
1.1	1000 cm^2	1.5	10 mm	3.41	2.98
1.2			7.5 mm	3.69	5.10
1.3			5 mm	4.43	11.56
1.4			10 mm	3.81	4.10
1.5		2.5	7.5 mm	4.27	7.14
1.6			5 mm	4.94	32.48
2.1	2000 cm^2	1.5	20 mm	3.20	0.86
2.2			10 mm	3.65	3.50
2.3			7.5 mm	4.09	5.08
2.4			20 mm	3.44	1.35
2.5		2.5	10 mm	4.26	3.98
2.6			7.5 mm	4.90	7.40

- Pressure drop in the porous graphite felt electrode

  For the pressure drop in the porous flow-through electrode, Darcy's law can be applied [21]:

$$\Delta p_{Eelectrode} = \frac{\mu_{El} h_E}{k_E w_E \delta_E} Q_C \tag{3.22}$$

  Where μ_{El} is the electrolyte dynamic viscosity [Pa s], h_E is the electrode height [m], k_E is the permeability of the porous electrode [m^2], w_E is the electrode width [m], δ_E is the electrode thickness [m] and Q_C is the cell volumetric flow rate [$m^3\ s^{-1}$].
  The permeability of the porous electrode, k_E, is derived using the Kozeny-Carman relation, as shown in Eq. (3.23):

$$k_E = \frac{d_F^2}{16 K_{KC}} \frac{\varepsilon_E^3}{(1-\varepsilon_E)^2} \tag{3.23}$$

  Where d_F is the fiber diameter of the graphite felt [m], K_{KC} is the Kozeny-Carman constant and ε_E is the porosity of the graphite felt electrode.

3.2 Regeneration process cost

The overall cost for the regeneration process can be expressed by the following equation:

$$C_{Regeneration\ Process} = C_{Power} + C_{Energy\ provided} + C_{pumping} \tag{3.24}$$

The only difference in respect to eq. (3.1) is that the energy costs, in this case, does not take into account the amount of electrolyte used in the system, because it comes from the VRFB, but it is related to the energy that has to be provided to recover the electrolyte.
Regarding the power cost and the pumping cost, all the equation described in chapter §3.1 can be applied also in the case of the regeneration system. But, two important main differences have to be taken into account: the first is the use of the DSA electrode for the positive side, which has a different material cost and fabrication cost respect to the graphite felt; the second is the cost of the stack expressed by the eq. (3.9). Here the active area (A_{Active}) is not an input parameter but depends on the current needed for the regeneration process. Therefore, the active area can be expressed by the following equation:

$$A_{Active} = \frac{i}{j} \tag{3.25}$$

Where *i* is the current [A] used for the regeneration and *j* is the current density [A/m^2] which has to be given as an input parameter (generally: j = 500-1000 A/m^2).

3.3 Numerical example

In order to make an example as close as possible to a real application, the dimension of the battery has been chosen by considering a typical energy demand for a single house

3.3.1 VRFB system costs

The single house considered for the example is a generic one, as shown in Fig. 3.3. In this house, solar panel are used to provide power during the day: this power is used both for the activities of the house and for charging the battery. A typical power demand for a single house is 5 kW and an energy demand is 15 kWh [22]. Therefore a 5 kW vanadium redox flow battery system with a storage time of 3 hours has been selected as example. All the data used for the economic model are reported in Tab. 3.3 [20]. A current density of 50 mA/cm^2 and an active area of 580 cm^2 are assumed. The number of the cells calculated through eq. (3.6) are 153 and the volume of the electrolyte calculated through eq. (3.13) is 0,688 m^3. The theoretical value of the standard potential differences is used as the reversible cell voltage (U_{Rev}), although the actual value can be higher due to membrane potentials [20]. Activation and concentration overvoltages are taken as constants in an initial approximation. The results are the following: the power-related cost is 39351 € and the energy-related cost is 6870 € and therefore the total cost is 46221 €.

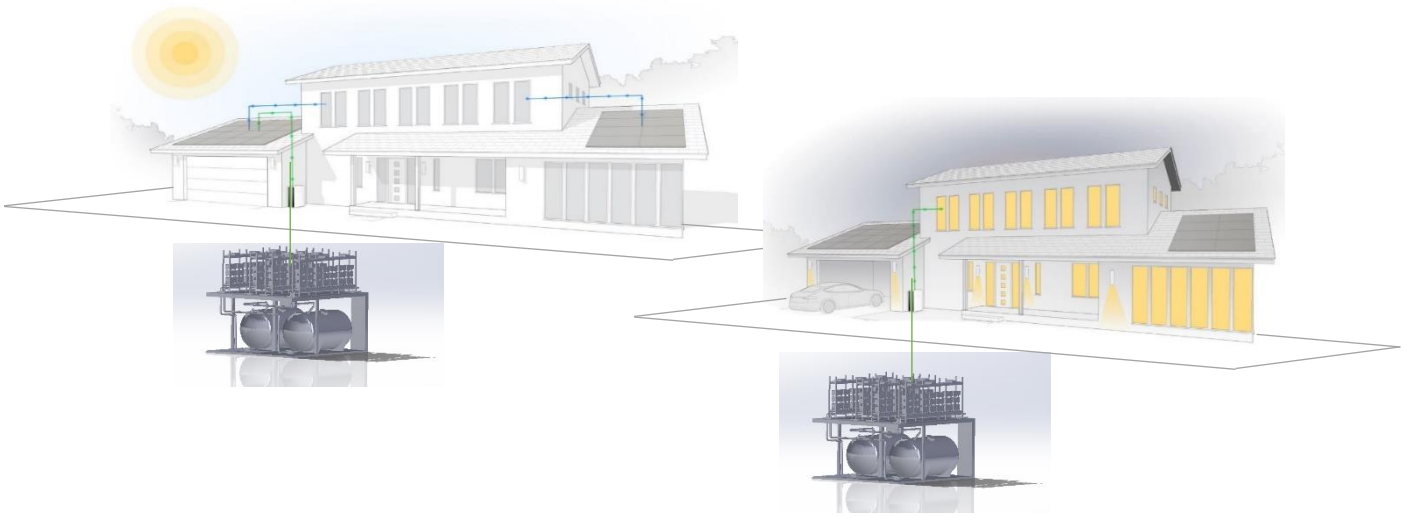

Figure 3.3: *Generic scheme of a house with solar panel: during the day the panels provide the energy necessary for the uses of the house and for charging the VRFB; during the night, only the battery provide the energy useful for the house.*

Table 3.3: *Input values for calculating the specific costs and cost distribution of a 5 kW/ 15 kWh vanadium redox flow battery [20].*

Parameter	Value	Unit	Parameter	Value	Unit
Mean power	10,000	W	Energy cost	0.3	€/kW
Storage time	12	h	Stack assembling energy	0.3	kWh/cell
Current density	50	mA/cm^2	System assembling	–	–
Active area	580	cm^2	Power cond. system cost	500	€/kW
Rev. cell voltage	1.255	V	Heat exchanger cost	1500	1/unit
Act. overpotential	0.005	V	Number of heat exchanger	2	unit
Conc. overpotential	0.02	V	Pump cost	1000	1/unit
Number of stacks	10	unit	Number of pumps	2	unit
Stack	–	–	Piping length	50	m
Membrane conductivity	1.44	S/m	Piping cost	20	€/m
Membrane cost	250	$€/m^2$	Number of valves	14	unit
Membrane factor	1.5		Valve cost	30	€/unit
Felt conductivity	83.3	S/m	Number of actuators	2	unit
Felt cost	150	$€/m^2$	Actuator cost	330	€/unit
Felt factor	1.5		Number of sensors	10	unit
BPP conductivity	5300	S/m	Sensor cost	250	€/unit
BPP cost	418	$€/m^2$	System assembling man hour	300	h
BPP factor	1.5	–	System assembling energy	1	kW/h
Gasket cost	392	$€/m^2$	Energy	–	–
Gasket fabr. cost	5	€/unit	Min theoretical SOC	0.2	–
Cell frame cost	100	$€/m^2$	Max theoretical SOC	0.8	–
Cell frame fabrication cost	5	€/unit	Tank cost	1.1	–
Current collector	700	$€/m^2$	Active species cost (Vanadium)	1.5	€/L
Current collector fabrication cost	5	€/unit	Active species concentration (Vanadium)	1.6	mol/L
Isolation plate cost	300	$300 €/m^2$	Solvent cost (H_2SO_4)	0.0083	€/mol
Isolation plate fabr. cost	20	€/unit	Solvent concentration (H_2SO_4)	2	mol/L
End plate cost	600	$€/m^2$	Additive 1 cost (H_3PO_4)	0.98	€/mol
Endplate fabr. cost	20	€/unit	Additive 1 conc. (H_3PO_4)	0.05	mol/L
Stack connection cost	3	€/unit	Electrolyte production cost	2.5	€/L
Stack assembling man hour	0.3	h/cell	–	–	–
Man hour cost	30	€/h	–	–	–

The cost for the pumping depends on the flowrate: by using the model described in the paragraph §3.1 it is possible to obtain the curve shown in Fig. 3.4. (See App. D for the Matlab script). In this example, the flow rate used for the battery is equal to 30 L/min; therefore, the pumping power is about 270 W. If this power is provided by the solar panel, it doesn't represent a cost for the house, otherwise, if it is taken from the grid, the costs is related to the energy cost of the specific country which the house belongs to. In this example the pumping power is provided by the solar panel.

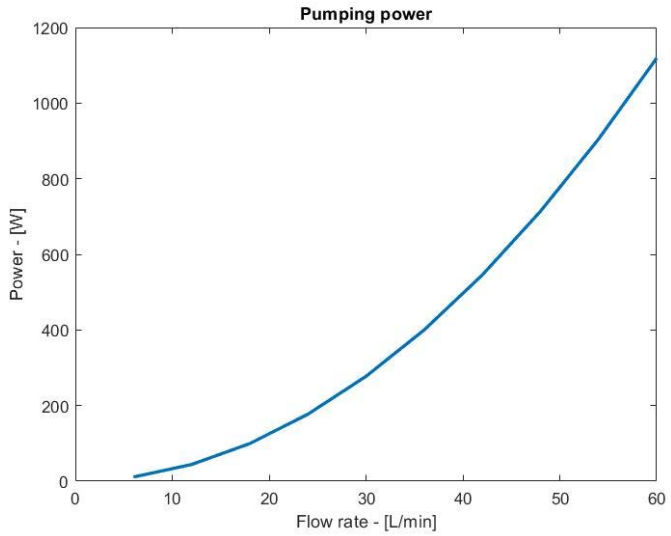

Figure 3.4: *Electric power demand for the VRFB considered in the numerical example.*

3.3.2 Regeneration system cost

The regeneration system cost has to be lower than the cost of the electrolyte used (in this case 4173 €) otherwise it is not convenient to regenerate it, as instead it would be cheaper buying new electrolyte. The total cost is divided in power costs, energy provided costs and pumping costs. Also in this case, the pumping costs are neglected because the power is provided directly by a renewable source. For the calculation of the power cost it is useful applying the following equation which does not depend on the power provided, but only on the active area.

$$C_{Power\ regen.} = \sum_i \left[(C_i * f_i) * Area + C_i^{Fabr} * n_i \right] \tag{3.26}$$

Where C_i is the price of the component, f_i is the material factor, C_i^{Fabr} is the fabrication costs and n_i is the number of units for the single cell. The single value used are presented in Tab.3.4. In this example a total current of 50A, provided to the regeneration system has been chosen. If a current density of 50 mA/cm^2 is assumed also in this system, the total active area resulted is equal to 0,1 m^2. Therefore, the power cost is equal to 2368 €. By using the mathematical model described in chapter §2, it is possible calculate the time requested for the regeneration: as shown in Fig. 3.5, after about 72 hours, the current reaches its maximum value and therefore the regeneration is complete. By applying a higher current, the time needed will decrease, but then the cost for the stack increases and the regeneration system become more expensive and not convenient anymore, as shown in Fig. 3.6.

Table 3.4: *Material costs and cost distribution of a 5 kW/ 15 kWh vanadium redox flow battery [20].*

	C_i - [€/unit]	f_i	C_i^{Fabr} - [€/unit]	n_i
Membrane	250	1.5	-	2
Graphite Felt	150	1.5	-	1
DSA	20 000	1	-	1
Bipolar plate	418	1.5	-	2
Gasket	392	1	5	2
Cell frame	100	1	5	2
Current collector	700	1	5	2
Isolation plate	300	1	20	2
End plate	600	1	20	2

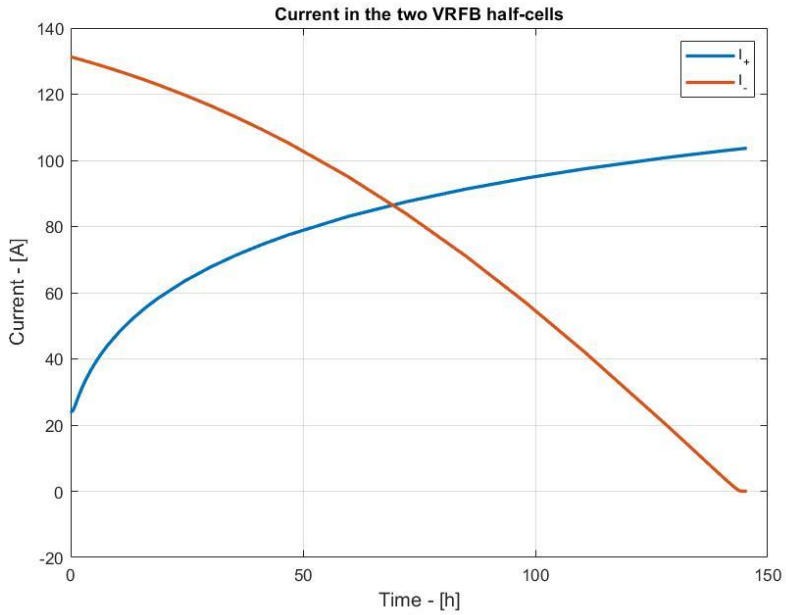

Figure 3.5: *Currents for the positive side and negative side of the VRFB when the current in the regeneration system equals to 50 A.*

In order to calculate the power and also the energy to provide to the system for the regeneration, the number of the cell has to be chosen. The total active area is 0,1 m^2; if each electrode has an area of 40 cm^2, the resulting cells number is 13. By considering the same effective voltage difference for a single cell as in the VRFB (1,128 V), the power which has to be released to the regeneration stack is 728 W. The source for this power can be the solar panel of the house if the regeneration process will take place during the day.

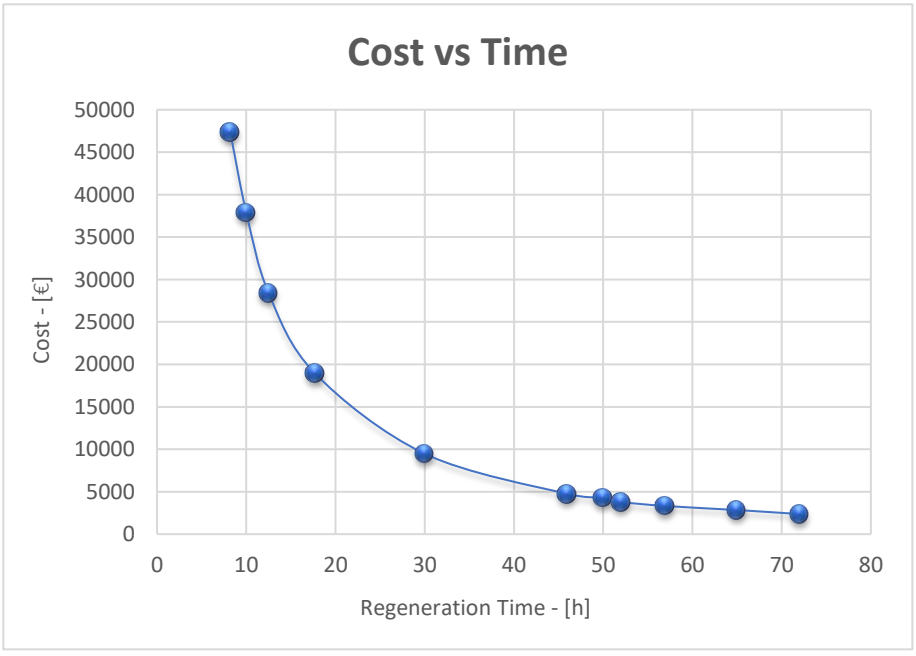

Figure 3.6: *Regeneration power costs as a function of the time for the regeneration.*

Table 3.5: *characteristics of the battery and of the regeneration system of the numerical example.*

		Power/Energy	Cost
VRFB	Power stack	5 kW	39351 €
	Energy	15 kWh	6870 €
	Pumping	0,270 kW	-
Regeneration system	Stack	-	2368 €
	Power demand	0,728 kW	-
Total			48589€

In Tab. 3.5 there are the main informations regarding the costs for the stack, for the electrolyte and for the pumping related to the VRFB system which has been selected in this work. Moreover, there are the power requested and the cost for building the stack of the regeneration system. The total cost is 42859 €. In this price the pumping cost for both the VRFB and the regeneration system and the cost of the energy to charge the battery have not been taken into account. The reason is that this energy is assumed to be provided by the solar panel of the house. Therefore, even though regenerating the electrolyte is convenient respect to buying new electrolyte, the problem are the batteries themselves. The VRFB are too expensive and too bulky compared with other technologies, such as the lithium-ion battery. A typical lithium-ion battery with the same power and energy demand as the one considered in the example, can cost around 7000 €, can make 10000 cycles of charge and discharge and the obstruction is very small [23]. Therefore, a lot of studies have to be carried out in order to improve the performance and specially to reduce the costs of this technology before to have a real commercialization.

Conclusion

This work of thesis has been dedicated to the study of a regeneration process for the electrolyte solution of vanadium redox flow batteries, focusing, on one hand, on the design as well as the characterization of the process itself and, on the other hand, on the material and operational costs of the technology.

The unbalance of the vanadium ions in the electrolyte has been solved by applying an electrochemical reactor. Here, the vanadium V^{+5} is reduced to V^{+4} which is fed back to the catholyte tank. During the charging operation, the V^{+4} in the catholyte allows the battery to reduced the V^{+3} in the anolyte which has been formed by side reactions. The reduction of V^{+5}, which takes place at the negative pole of the regeneration reactor, is made possible through a simultaneous oxidation at the positive pole where a specific electrode is used, made with Titanium and Iridium Oxide.

The characterization of the process has been conducted through the use of direct experiments and of mathematical modelling. Thanks to the experiments it has been possible seeing the dynamic response of the battery when the electrolyte regeneration is applied. The response shows a current profile where a maximum point is observed, which can be justified from a physical point of view: it is the point where the concentration of reduced and oxidised species in the anolyte and catholyte are balanced again. This has been confirmed by the mathematical model which has been obtained by resolving all the ordinary differential equations which describe the mass balances both for the vanadium redox flow battery and the regeneration reactor. The solution of the model well described the current behaviour of the experiments and, therefore, it confirms that a suitable end-point criterion for the recovery process is the point in which the current in the battery shows its maximum value.

The economic analysis, instead, was necessary in order to understand if the regeneration process can be competitive compared to other methods of rebalancing the species in the electrolyte. The analysis, through a numerical example, provides the cost of the regeneration process for a 5 kW-10 kWh vanadium redox flow battery system: the cost is 2368 €. Moreover, through a mathematical model, the time needed for the regeneration has been calculated to be between 50-70 hours. With a faster regeneration process, the operational and capital costs increase and the recovery of the electrolyte is not convenient anymore, e.g. compared to buying new electrolyte.

The problem which emerges from this study is the way to measure, easily and accurately, the imbalance between the reduced and oxidised species in the electrolyte, before applying the regeneration reactor.

Therefore, future studies will have to face this problem in order to better understand both the effect of the imbalance on the performance of the battery along the time and the right time to apply the regeneration process.

Finally, in order to make the recovery process faster and easier other experiments have to be conducted, especially on a real scale, which means to use not a single cell for the regeneration, as done in this work, but a stack of cells and observing how the response of a plant of battery changes during the time.

Appendix A

Script of Matlab for the solution of the ODEs (2.38-47)

```
%%%%%%%%%%%%%%%%%%%%%%%%%%%%%%%%%%%%%%%%%%%%
%%%%%%% Electrochemical process %%%%%%%%%
%%%%%%%%%%%%%%%%%%%%%%%%%%%%%%%%%%%%%%%%%%%%

% Vanadium(5)_tank = A
% Vanadium(4)_tank = B

% Vanadium(5)_cell = C
% Vanadium(4)_cell = D

% Vanadium(5)_dsa = E
% Vanadium(4)_dsa = F


% Vanadium(3)_tank = A
% Vanadium(2)_tank = B

% Vanadium(3)_cell = C
% Vanadium(2)_cell = D


%% Function to solve Mass Balance (ODE)

function DSAregeneration_shift_20


XA0 = 1.624*0.999*10^(3);    % Intial concnetration of V5 in the positive tank, [mol/m^3]
XB0 = 1.624*0.001*10^(3);    % Intial concnetration of V4in the positive tank, [mol/m^3]

XC0 = 1.6*0.999*10^(3);      % Intial concnetration of V5 in the cell, [mol/m^3]
XD0 = 1.6*0.001*10^(3);      % Intial concnetration of V4 in the cell, [mol/m^3]

XE0 = 1.624*0.999*10^(3);    % Intial concnetration of V5 in the DSA, [mol/m^3]
XF0 = 1.624*0.001*10^(3);    % Intial concnetration of V4 in the DSA, [mol/m^3]

XG0 = 1.624*0.20*10^(3);     % Intial concnetration of V3 in the negative tank, [mol/m^3]
XL0 = 1.624*0.80*10^(3);     % Intial concnetration of V2 in the negative tank, [mol/m^3]

XM0 = 1.624*0.20*10^(3);     % Intial concnetration of V3 in the cell, [mol/m^3]
XN0 = 1.624*0.80*10^(3);     % Intial concnetration of V2 in the cell, [mol/m^3]


X0 = [XA0;XB0;XC0;XD0;XE0;XF0;XG0;XL0;XM0;XN0];    % initial condition vector



%% ODE
[z,X] = ode15s(@MBi,[0 72000],X0);



%%
%%%%%%%%%%%%%%%%%%%%%%%%
%%%%%%% PLOTS %%%%%%%%%
%%%%%%%%%%%%%%%%%%%%%%%%


xA = X(:,1);  % concentration of V5 in the positive tank
xB = X(:,2);  % concentration of V4 in the positive tank

xC = X(:,3);  % concentration of V5 in the cell
xD = X(:,4);  % concentration of V4 in the cell

xE = X(:,5);  % concentration of V5 in the dsa
xF = X(:,6);  % concentration of V4 in the dsa

xG = X(:,7);  % concentration of V3 in the negative tank
xL = X(:,8);  % concentration of V2 in the negative tank

xM = X(:,9);  % concentration of V3 in the cell
```

```
xN = X(:,10); % concentration of V2 in the cell

z = z/3600;    % trasform second in hour for the plots


%% Composition of V5,V4;V3,V2 in the positive and negative tank

figure(1)

plot(z,xA,'linewidth',2)
hold on
plot(z,xB,'linewidth',2)
plot(z,xG,'linewidth',2)
plot(z,xL,'linewidth',2)

title('Concentration in the positive and negtive tank')
xlabel('Time - [min]')
ylabel('Concentration - [mol/m^3]')
legend('C_V_5','C_V_4','C_V_3','C_V_2')
hold off

%% Composition of V5,V4;V3,V2 in cell

figure(2)

plot(z,xC,'linewidth',2)
hold on
plot(z,xD,'linewidth',2)
plot(z,xM,'linewidth',2)
plot(z,xN,'linewidth',2)

title('Concentration in the cell')
xlabel('Time - [min]')
ylabel('Concentration - [mol/m^3]')
legend('C_V_5','C_V_4','C_V_3','C_V_2')
hold off

%% Composition of V5,V4 in the regeneration reactor

figure(3)
plot(z,xE,'linewidth',2)
hold on
plot(z,xF,'linewidth',2)

title('Concentration in the Regeneration reactor')
xlabel('Time - [min]')
ylabel('Concentration - [mol/m^3]')
legend('C_V_5','C_V_4')
hold off


 %% Three SUBPLOT

figure(4)


% (1) subplot: conenctration of V5 and V4 in the positive tank
subplot(1,3,1)
plot(z,xA,'linewidth',2)
title('Concentration in the Catholyte')
xlabel('Time - [min]')
ylabel('Concentration - [mol/m^3]')
hold on
plot(z,xB,'linewidth',2)
legend('C_V_5','C_V_4')
hold off

% (2) subplot: Current in the cell
subplot(1,3,2)

i_p = (n*F*K0_C*E_p*Area).*(xC.^(1-alpha).*xD.^alpha);   % Current in the positive half-cell [A]
i_n = (n*F*K0_N*E_n*Area).*(xM.^(1-alpha).*xN.^alpha);   % Current in the negative half-cell [A]


plot(z,i_p,'linewidth',2)
title('Current in the VRFB half-cells')
xlabel('Time - [min]')
ylabel('Current - [A]')
```

```
hold on
plot(z,i_n,'linewidth',2)
hold off
legend('I_+','I_-')



% (3) subplot: Concentration of V3 and V2 in the Negative Tank
subplot(1,3,3)
plot(z,xG,'linewidth',2)
hold on
plot(z,xL,'linewidth',2)

title('Concentration in the Anolyte')
xlabel('Time - [min]')
ylabel('Concentration - [mol/m^3]')
legend('C_V_3','C_V_2')

hold off


%% Comperison between the current in the cell an the concentration of V4 and V3

figure(5)

% (1) subplot: conenctration of V4 and V3 in the positive tank
subplot(2,1,1)
plot(z,xD,'--','linewidth',2)
hold on
plot(z,xM,'--','linewidth',2)
title('Concentration of V^4^+ in the catholyte and of V^3^+ in the anolyte ')
xlabel('Time - [h]')
ylabel('Concentration - [mol/m^3]')
legend('C_V_4','C_V_3')

hold off


% (2) subplot: Current in the cell

subplot(2,1,2)
plot(z,i_p,'linewidth',2)
hold on
plot(z,i_n,'linewidth',2)
% plot(z,y,'linewidth',2)
title('Current in the two VRFB half-cells')
xlabel('Time - [h]')
ylabel('Current - [A]')
legend('I_+', 'I_-')

hold off


%% Different dynamics: comperison between concentration of V4 in the cell and in the reactor

figure(6)
plot(z,xF,'linewidth',2)
hold on
plot(z,xD,'linewidth',2)
hold off
title('Concentration of V^4^+ in the Reactor and in the Cell')
xlabel('Time - [h]')
ylabel('Concentration - [mol/m^3]')
legend('C_V_4^R','C_V_4^C^e^l^l')

end


%%%%%%%%%%%%%%%%%%%%%%%%%%%%%%%%%%%%%%%%
%%%%%%%%%%%%%%%%%%%%%%%%%%%%%%%%%%%%%%%%
%%%%%%% END PLOTS %%%%%%%%%%%%%%%%%%%%%
%%%%%%%%%%%%%%%%%%%%%%%%%%%%%%%%%%%%%%%%
%%%%%%%%%%%%%%%%%%%%%%%%%%%%%%%%%%%%%%%%

%% Mass Balances

function dXdz = MBi(z,X)
```

```
XA = X(1); % concentration of V5 in the positive tank
XB = X(2); % concentration of V4 in the positive tank

XC = X(3); % concentration of V5 in the cell
XD = X(4); % concentration of V4 in the cell

XE = X(5); % concentration of V5 in the DSA
XF = X(6); % concentration of V4 in the DSA

XG = X(7); % concentration of V3 in the negative tank
XL = X(8); % concentration of V2 in the negative tank

XM = X(9); % concentration of V3 in the Cell
XN = X(10); % concentration of V2 in the Cell


%% COSTANTS

alpha = 0.45;            % electron transfert coefficient, [adim]
n = 1;                   % number of electron exchange in the reaction, [adim]
F = 96485;               % Faraday constant, [coulomb/mol]
SOC_p = XC/(XC+XD);
eta_p = 1.65 - 1.255 + 0.07 + 0.059 * log ((SOC_p/100/(1 - SOC_p/100 )*(3.4 + SOC_p/100* 1.6
))^2*((3.4 + SOC_p/100* 1.6 )/( 1.8 + SOC_p/ 100*1.6)));              % Overpotential+, [V]
SOC_n = XN/(XM+XN);
eta_n = 1.65 - 1.255 + 0.07 + 0.059 * log ((SOC_n/100/(1 - SOC_n/100 )*(3.4 + SOC_n/100* 1.6
))^2*((3.4 + SOC_n/100* 1.6 )/( 1.8 + SOC_n/ 100*1.6)));              % Overpotential-, [V]
R = 8.31;                % Gas costant, [J/(mol*K)]
T = 293.15;              % Temperature, [K]
K0_C = 3.5*10^(-8);      % Cathodic kinetic constant, [m/s]
K0_N = 7.2*10^(-8);      % Cathodic kinetic constant, [m/s]
Area = 0.0040;            % Area of electrode, [m^2]
V = 8*10^(-5);           % Volume of electrolye, [m^3]
V_flow = 1.67*10^(-6);   % Volumetric flow rate, [m^3/s]
tau = V/V_flow;          % time constant [s]
K = 1/(V_flow*F);        % costant for generation term in mass balance
E_p = exp(((alpha)*n*F*eta_p)/(R*T))- exp(-(alpha*n*F*eta_p)/(R*T));   % Butler Volmer exponential
term, [adim]
E_n = exp(((alpha)*n*F*eta_n)/(R*T))- exp(-(alpha*n*F*eta_n)/(R*T));   % Butler Volmer exponential
term, [adim]


%% Current in Positive tank
j0_p = n*F*K0_C*(XC*XD)^alpha;      % Exchange current density, [A/m^2]
j_p = j0_p*E_p;                     % Current density, [A/m^2]
i_cell_p = j_p*Area;                % Current, [A]


%% Current in Negative tank
j0_n = n*F*K0_N*(XM*XN)^alpha;      % Exchange current density, [A/m^2]
j_n = j0_n*E_n;                     % Current density, [A/m^2]
i_cell_n = j_n*Area;                % Current, [A]

%% DSA current
i_dsa = 1;                          % current in the DSA, [A]


%% Equazioni differenziali

dXAdz = (-2*XA + XE + XC)/tau;              % Differential equation for V5 in the Tank
dXBdz = (-2*XB + XF + XD)/tau;              % Differential equation for V4 in the Tank

dXCdz = (XA - XC + K*i_cell_p)/tau;         % Differential equation for V5 in the Cell
dXDdz = (XB - XD - K*i_cell_p)/tau ;        % Differential equation for V4 in the Cell

dXEdz = (XA - XE - K*i_dsa)/tau;      % Differential equation for V5 in the DSA
dXFdz = (XB - XF + K*i_dsa)/tau;      % Differential equation for V4 in the DSA

dXGdz = (XM - XG)/tau;                % Differential equation for V3 in the Tank
dXLdz = (XN - XL)/tau;                % Differential equation for V2 in the Tank

dXMdz = (XG - XM - K*i_cell_n)/tau;      % Differential equation for V3 in the Cell
dXNdz = (XL - XN + K*i_cell_n)/tau;      % Differential equation for V2 in the Cell

dXdz = [dXAdz; dXBdz; dXCdz; dXDdz; dXEdz; dXFdz; dXGdz; dXLdz; dXMdz; dXNdz ];

end
```

Appendix B

Spectrometric state of charge determination for the negative half-cell of the VRFB

The state of charge of the anolyte has been measured with a UV/Vis spectrometer (HR2000+, Ocean Optics, USA). Through this spectrometer, the UV/Vis spectra have been recorded in-situ during the charging. The absorbance maxima are attributed to d-d transitions, with comparatively low intensity. The 2D experimental results are displayed in Fig. 1: each spectrum depends on the composition of V^{2+} and V^{3+}. When the concentration of V^{3+} is 99,5 %, two maxima are observed: one at 400 nm and the other one at 600 nm. But, as the state of charge increases, namely the concentration of V^{2+} increases, a continuous decrease of the absorbances of both peaks is observed. This decrease is found to be more pronounced for the absorbance band at 400 nm. Simultaneously a peak at 570 nm is evolving and a low-intensity maximum of the V^{2+} species at 850 nm, with steadily increasing absorbance.

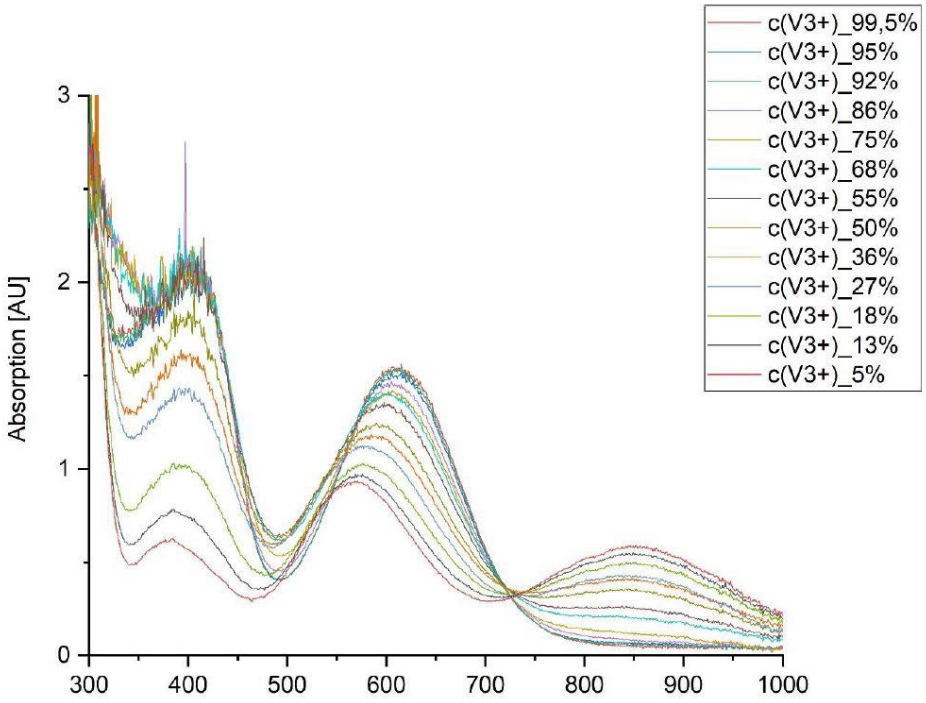

Figure 1: *Negative half-cell electrolyte (anolyte): In-situ UV/Vis spectral data as function of absorbance length and parametric respect to the concentration of V^{3+}.*

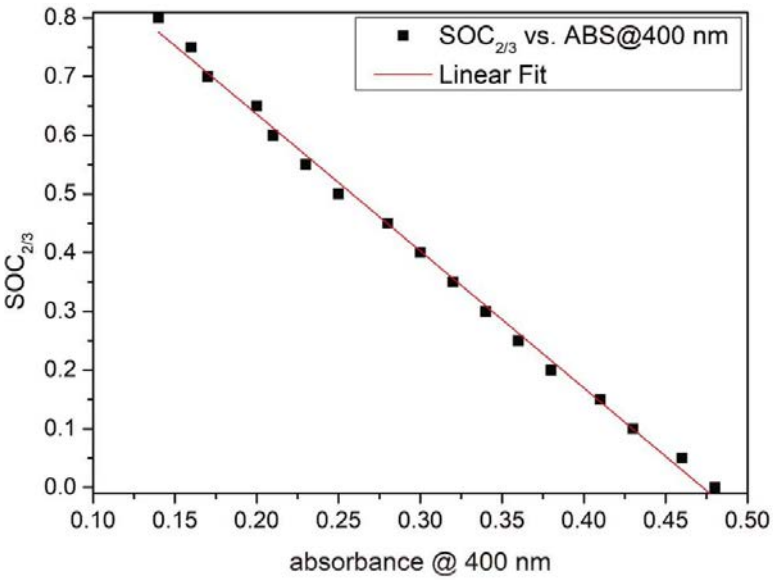

Figure 2: *Negative half-cell electrolyte (anolyte): Linear fit of the measured absorbance values at 400 nm as function of the $SOC_{2/3}$ (according to OCV cell voltage). [22]*

Due to the stronger signal at low states of charge in combination with a more pronounced decrease in signal intensity with rising the state of charge, the absorbance maximum for V^{3+} at 400 nm can be used for the photometric analysis of the state of charge of the anolyte: as displayed in Fig. 2, the measured absorbance values (abs) at 400 nm depend linearly on the $SoC_{2/3}$ according to:

$$SOC_{2/3}(abs) = 1.10 - 2.33 * abs\ (@\ 400\ nm)$$

Through this equation it is possible to calculate the SoC of the anolyte. In the balanced electrolyte, the state of charge of the anolyte is equal to the state of charge of the catholyte.

Appendix C

Effective cell voltage

The working principle of redox-flow batteries can be described as a chemical reaction of two redox couples that result from the combination of two corresponding half-cell reactions, as follows:

Anode :	A^x	$\rightarrow A^{x+z} + ze^-$	φ_A
Cathode :	$C^y + ze^-$	$\rightarrow C^{y-z}$	φ_C
Cell :	$A^x + C^y$	$\rightarrow A^{x+z} + C^{y-z}$	$U_{rev} = \varphi_C - \varphi_A$.

As one important factor, the ohmic losses of a stack reduce the efficiency of the battery. The standard open circuit voltage (U_{rev}) can be calculated by the Nernst equation as follows:

$$U_{rev} = \left(\phi_C^0 - \phi_A^0\right) + \frac{RT}{zF}\ln\left(\frac{C_{C,ox} * C_{A,red}}{C_{C,red} * C_{A,ox}}\right) \quad (1)$$

where ϕ_C^0 and ϕ_A^0 are the standard redox potentials for the reaction at the positive and negative electrodes, R as the universal gas constant, T the temperature, and cox and cred are the molar concentration of the oxidant and reductant. Since a cell has different kinds of losses, the effective cell voltage is calculated as the reversible cell voltage subtracted by all losses inside the cell [20]:

$$U_{cell} = U_{rev} - U_{act} - U_{con} - U_{ohm} \quad (2)$$

where U_{act} is the activation overpotential, U_{con} is the concentration overpotential, and U_{ohm} is the ohmic overpotential. The non-linear response of the overpotential U_{act} with the current density can be taken into account using the Butler–Volmer equation, although this requires a knowledge of the material-dependent exchange current densities i_0 and the symmetry factors α (or β) for reactions in a complete cell or cell stack. Chen et al. calculated them with Equations (3) and (4), although it must be remembered that the symmetry factor α and the exchange current density i_0 are strongly electrode material dependent and usually not the same for the charge and discharge process [20].

$$U_{act} = \alpha\ln\left(\frac{i}{i_0}\right) \quad (3)$$

$$U_{con} = \frac{RT}{zF}\ln\left(\frac{i_L}{i_L - i}\right) \quad (4)$$

Since α, i_0 , and the limiting current density i_L are difficult to obtain, U_{act} and U_{con} were left as constants in an initial approximation so as to be able to supplement the model with measured values later. The overpotentials result in all cases in heat generation, which means a loss in energy and lower battery efficiency. The ohmic losses consist of material resistances and contact resistances between the different cell components. As the choice of component directly influences the ohmic losses, this part is described in more detail with Equations (5) and (6):

$$U_{ohm} = i * \left(R_{Membrane} + 2 * R_{Felt} + R_{BPP} + R_{Contact} + R_{Electrolyte}\right) \quad (5)$$

$$U_{ohm} = i * \left(\frac{b_{Membrane}}{A_{Active} * \sigma_{Membrane}} + \frac{b_{Felt}}{A_{Active} * \sigma_{Felt}} + \frac{b_{BPP}}{A_{Active} * \sigma_{BPP}} + R_{Contact} + R_{Electrolyte}\right) \quad (6)$$

where b is the thickness, σ is the specific conductivity, A_{Active} is the active cell area, and R is the ohmic resistance. As the felt electrode is soaked with electrolyte, the conductivity will be different from the felt-only conductivity. This formula directly relates cell material performances and the current to ohmic losses. It can be seen that the ohmic losses are a function of the electric current. For this reason, the effective cell voltage can only be calculated when the current is known. Contact and electrolyte resistances were treated as constants. The resistance values for membrane, felt, and bipolar plate were broken down by thickness and specific conductivity and made scalable by a reference to the active surface area. As the voltage is a function of the state of charge (SoC)/depth of discharge (DoD), the average cell voltage has to be calculated in the used SoC range. The effective stack voltage is calculated as the sum of the effective cell voltages [20]:

$$\overline{U_{cell}} = \frac{1}{SoC_{max} - SoC_{min}} \int_{SoC_{min}}^{SoC_{max}} U_{cell} dSoC \quad (7)$$

$$\overline{U_{stack}} = \sum_{n=1}^{N} \overline{U_{cell,n}} \quad (8)$$

Appendix D

Script of Matlab for the pump power calculation

```
%%% PUMP POWER CALCULATION %%%

clear all, clc

mu = 4.928*10^(-3);                              % Electrolyte dynamic viscosity  [Pa*s]
h = 0.3;                                         % Electrode hight [m]
df = 30*10^(-5);                                 % Fiber diameter of the graphite felt [m]
Kkc = 4.28;                                      % Kozeny-Carman constant [-]
epsilon = 0.93;                                % Porosity of the graphite felt electrode [-]
k = (df^2)*(epsilon^3)/(16*Kkc*(1-epsilon)^2); % Permeability of the porous electrode
[m^2]
w =0.02 ;                                        % Electrode width [m]
sigma = 0.05 ;                                   % Electrode thickness [m]

alpha = (mu*h)/(k*w*sigma);
beta = 3.41*10^(-7);                             % coefficient [Pa*s*m^(-3)]
gamma = 2.98*10^(-9);                            % coefficient [Pa*(s*m^(3))^2]

rho = 1.345;                                     % Electrolyte density [kg/m^3]


Qori = [0:0.0001:0.001];                       % Volumetric flowrate of the orifice  [m^3/s]
Qp = Qori;                                     % Volumetric flowrate of the pipe [m^3/s]
Qc = Qp;                                       % Volumetric flowrate of the channels [m^3/s]

N_cell = 150 ;                                     % Number of the cell
Lp = 5;                                            % Lentgh of the pipes [m]
dp = 0.03;                                         % Pipe diameter [m]
dori = 0.005;                                      % Orifice diameter [m]
Kl = 0.7;                                      % Loss coefficient for hydraulic elements [-]
Re = 4*(rho*Qp)/(mu*pi*dp);                        % Reynolds number [-]
f = 64./Re;                                        % Friction Factor [-]


%% Pressure drops

deltaP_stack = ((alpha + beta)*Qc + gamma*Qc.^2)*N_cell

deltaP_pipe = 8*f*Lp*rho.*(Qp.^2)/((pi^2)*(dp^5))

deltaP_orifice = 4*(8*Kl*rho.*(Qori.^2)/((pi^2)*(dori^4)))

deltaP = deltaP_stack + deltaP_pipe + deltaP_orifice;

eta = 0.50;                     % Efficiency of the pump
P = 2*deltaP.*Qp./(eta);        % Pump power
Q = Qori*1000*60;               % Volumetric flowrate [L/min]

%% Plots

plot(Q,P,'linewidth',2)   % Power as function of the volumetric flowrate
title('Pumping power')
xlabel('Flow rate - [L/min]')
ylabel('Power - [W]')
```

Appendix E

Optical ICP Emission Spectrometry

Through the ICP-OES measurement it is possible observing that there is no residuals of Iridium Oxide and Titanium in the electrolyte.
In Fig. 1, in fact, there are shown two different measurements: the green column represents the electrolyte solution before the interaction with the DSA electrode and the blue one, instead, represents the electrolyte solution after the regeneration and therefore after the interaction with the dimensional stable anode. Since the concentration is the same before and after the recovery, it means that the Titanium and the Iridium Oxide of the DSA electrode are stable on the surface of the it.
If there were some leaks of both Iridium Oxide and Titanium, they would catalyse side reactions in the battery and therefore they would compromise its energy capacity.

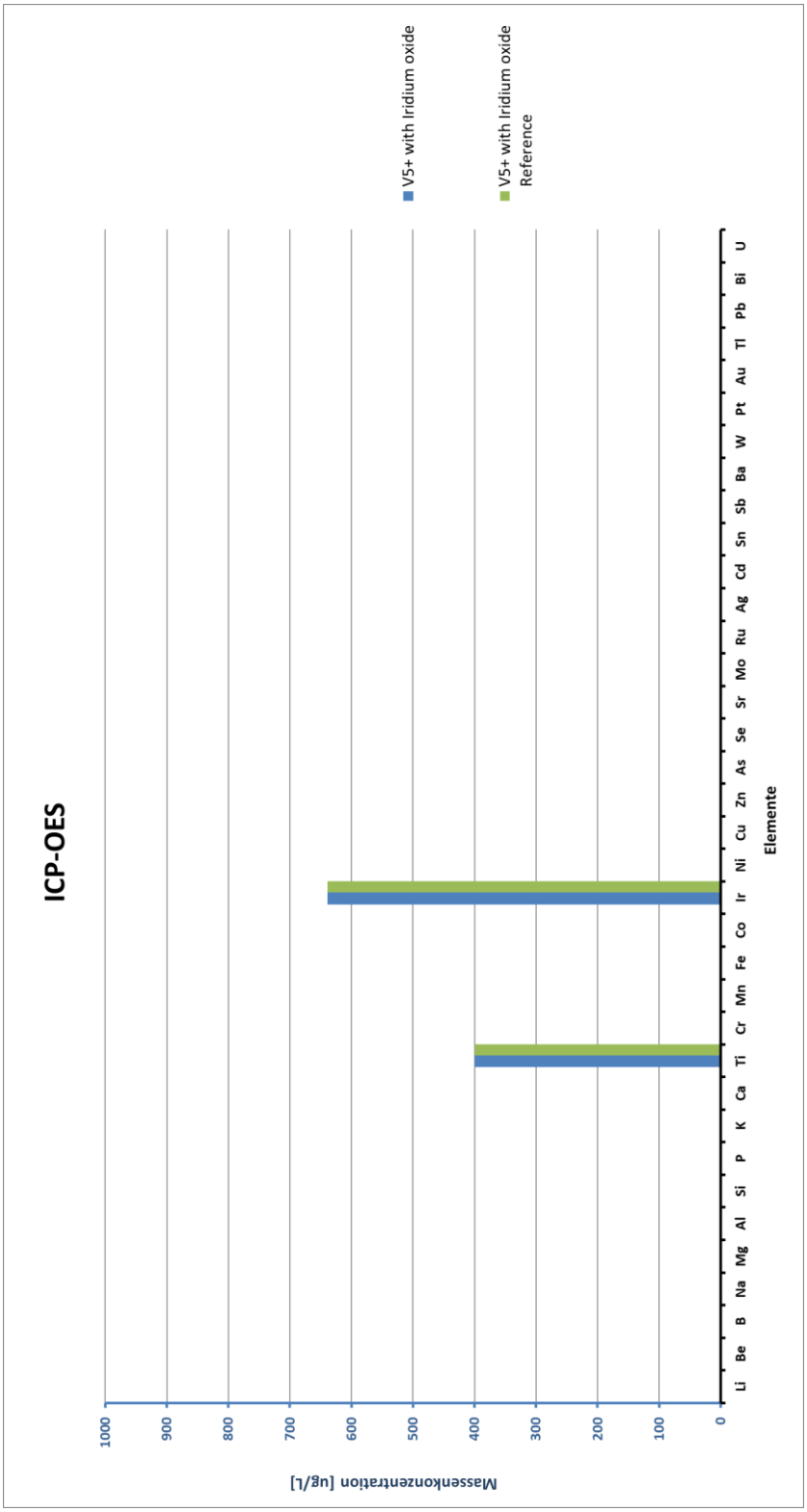

Figure 1: *ICP-OES measurements: the concentration of Titanium and Iridium Oxide in the electrolyte before and after the regeneration process is the same; no leaks from the electrode.*

Appendix F

Notation

α	Transfer coefficient
A	Area
A_{active}	Active area
β	Hydraulic resistance coefficient
C	Unit cost
c	Specific cost
c_i	Concentration of species i
δ	Electrode thickness
d_p	Pore diameter
d_c	Channel diameter
d_p	Pipe diameter
E^0	Standard potential
E_{eq}	Equilibrium potential
φ_s	Electric potential of the solid phase
φ_e	Electrolyte potential
F	Faraday constant
h	Electrode high
i	Current
i_0	Exchange current density
j	Current density
k_+	Cathode kinetic constant
k_-	Anode kinetic constant
k	Permeability of the porous electrode
k_{KC}	Kozney-Carman constant
l	Pipe length
μ	Electrolyte dynamic viscosity
N_i	Molar flow rate
P	Power
p	pressure
Q	Volumetric flow rate
ρ	Density
R	Gas constant
T	Temperature
U_{cell}	Cell overpotential
U_{con}	Concentration overpotential
U_{act}	Activation overpotential
U_{ohm}	Ohmic overpotential
U_{rev}	Standard open circuit voltage
V	Volume

References

1. World Energy Outlook 2011, International Energy Agency; 2011. (http://www.worldenergyoutlook.org).
2. Annual Energy Outlook 2012 Early Release Overview , U.S. Energy Information Administration; 2012. (http://www.eia.gov/forecasts/aeo/er).
3. European Commission,Proposal for a COUNCIL DECISION establishing the Specific Programme Implementing Horizon2020—The Framework Pro- gramme for Research and Innovation (2014–2020), COM(2011)811 final, 2011/0402(CNS).
4. Swierczynski M, Teodorescu R, Rasmussen CN, Rodriguez P, Vikelgaard H. Overview of the energy storage systems for wind power integration enhance- ment. In: Proceedings of the IEEE international symposium on industrial electronics (ISIE 2010), 3749-3756, 2010.
5. Vazquez S, Lukic S, Galvan E, Franquelo LG, Carrasco JM, Leon JI. Recent advances on energy storage systems. In: Proceedings of the IECON 2011: 37th annual conference of the IEEE industrial electronics society, 4636-4640, 2011.
6. Ren L, Tang Y, Shi J, DouJ , Zhou S, Jin T. Techno-economic evaluation of hybrid energy storage technologies for a solar-wind generation system. Physica C: Superconductivity 2013; 484:272–5.
7. Zahedi A. Maximizing solar PV energy penetration using energy storage technology. Renewable and Sustainable Energy Reviews 2011; 15:866–70.44.
8. P. Alotto, M. Guarnieri, F. Moro. Redox flow batteries for the storage of renewable energy: a review. Renewable and suitable energy reviews 29 (2014) 325-335.
9. Dunn B, Kamath H, Tarascon J. Electrical energy storage for the grid: a battery of choices. Science 2011; 334:928–35.
10. Yang Z, Zhang J, Kintner-Meyer MC W, Lu X, Choi D, Lemmon JP, Liu J. Electrochemical Energy Storage for Green Grid. Chemical Reviews 2011; 111:3577–613.
11. Leung P, Li X, de Leon C, Berlouis L, Low J. Progress in redox flow batteries, remaining challenges and their applications in energy storage. RSC Advances (2012), 2, 10125-10156.
12. Ding C, Zhang H, Li X, Liu T, Xing F. Vanadium flow battery for energy storage: prospects and challenges. J. Phys. Chem. Lett. 2013, 4, 1281-1294.
13. Skyllas-Kazacos M, Kazacos M. State of charge monitoring methods for vanadium redox flow battery control. J. Power Sources 196 (2011) 8822-8827.
14. Rudolph S, Schroder U, Bayanov I.M. On-line controlled state of charge rebalancing in vanadium redox flow battery. J. Electroanalytical Chemistry 703 (2013) 29-37.
15. Roznyatovkaya N, Herr T, Kuttinger M, Fuhl M, Noack J, Pinkwart K, Tubke J. Detection of capacity imbalance in vanadium electrolyte and its electrochemical regeneration for all-vanadium redox flow batteries. J. Power Source 302 (2016) 79-83.
16. Wang J, Zhong H, Qin Y. Zhang X. An efficient three-dimensional oxygen evolution electrode. Angew. Chem. Int. 2013, 52, 5248-5253.
17. Shah A, Watt-Smith M.J, Walsh F.C. A dynamic performance model for redox-flow batteries involving soluble species.
18. Blanc C, Rufer A. Understaning the Vanadium Redox Flow Batteries. Ecole Polytechnique Federal de Lausanne Switzerland.
19. Schreiber M, Harrer M. Lifetime of vanadium redox flow batteries. Cellstrom GmbH, IZNO-Sud Wr. Neudorf, Austria.

20. Noack J, Wietschel L, Roznyatovskaya N, Pinkwart K, Tubke J. Techno-Economic Modeling and Analysis of Redox Flow Battery System. Energies 2016, 9, 627. Fraunhofer-Institue for Chemical Technology.
21. Konig S. Model-based design and optimization of vanadium redox flow batteries.
22. Geiser J, Natter H, Hempelmann R. Photometrical determination of the state of charge in vanadium redox flow batteries.Part II: in combination with open circuit voltage. Z. Phys. Chem. 2009.
23. Website: https://luce-gas.it/guida/contatore/potenza
24. Website: https://www.tesla.com/it_IT/powerwall